



# Alkyl sucrose esters vs. Brijs: How chain length and temperature impact surface and foam properties

L. Delforce, S. Tcholakova\*

Department of Chemical Engineering, Sofia University, Sofia, Bulgaria

## ARTICLE INFO

### Keywords:

Foam  
Sucrose ester  
Brij  
Surface coverage  
Bartsch test  
Foam rise method  
Planetary mixer  
Shear-thinning  
Worm-like micelles

## ABSTRACT

The primary objective of this study is to determine the similarities and differences in the surface, film, and foam properties of alkyl sucrose esters (SEs) with high monoester content ( $\geq 70\%$ ) and polyoxyethylene alkyl ethers (Brijs) with a high number of ethoxy groups ( $\geq 20$ ) in their head group. Experiments were conducted using surfactant molecules with alkyl chain lengths of 12, 16, and 18 carbon atoms at concentrations between 0.01 and 1 wt%, within a temperature range of 25 °C to 60 °C.

The lag time for surfactant adsorption increased with surfactant chain length, decreased with temperature, and significantly decreased with surfactant concentration for both types of studied surfactants. However, increasing the chain length from 12 to 18 carbon atoms led to a 10-fold increase in lag time for Brijs and more than a 600-fold increase for SEs. This effect rendered longer-chain SEs incapable of forming voluminous foam in Bartsch test and led to pronounced coalescence between the bubbles after their separation from the sparger in the foam rise method, resulting in foams with very large bubbles, which exhibited lower stability. The utilization of a Kenwood mixer for foam generation provided sufficient time for longer-chain SE molecules to adsorb on the bubble surfaces and to produce voluminous foams with small bubbles, which remained stable even at 60 °C. In contrast, foams generated from Brijs solutions are very unstable at 60 °C. The long-standing stability of SEs foam was attributed to the formation of mixed mono- and diesters adsorption layers on the bubble surfaces.

## 1. Introduction

Foams are widely studied in the literature due to their importance for various technologies such as enhanced oil recovery [1–5], food industry [6–8], pulp and paper production [9], and formation of polymeric and inorganic solid foams for thermal isolation [10–15], etc.. Foams are thermodynamically unstable and surfactants are usually added in the solutions for their stabilization. Most of the currently used surfactants are synthesized from fossil resources, which have a significant footprint. There is currently a need to substitute these surfactants with more eco-friendly ones. One class of these surfactants is sucrose alkyl esters, synthesized from sucrose and fatty acids, both produced from non-fossil ingredients.

Sucrose alkyl esters, recognized for their biodegradability and biocompatibility, are widely utilized in the food industry [16–19]. They contain a mixture of mono-, di-, and triesters, the ratios of which affect the foam properties [20]. In a commercially available mixture of sucrose laurate (L1695) enhanced foamability and stability was observed

compared to individual sucrose monolaurate or sucrose dilaurate [20]. This is attributed to the initial fast adsorption of sucrose monolaurate at the surface followed by progressive adsorption of sucrose dilaurate and formation of a mixed adsorption layer [21]. The alkyl chain length in sucrose esters also impacts their foaming properties: Nelen *et al.* reported decreasing foamability in the Ross-Miles method with increasing the alkyl chain length in sucrose esters with HLB values of 15–16, assuming equilibrium surface tension values were responsible for this tendency [17]. Poorer foamability in a shaken cylinder was also reported for pure palmitate sucrose ester compared to caprate and laurate ones [18]. For fructose monoesters, foamability in Ross-Miles test was shown to decrease with the increase of chain length from 14 to 18 [22]. Similar results were reported for sucrose esters with chains between C<sub>12</sub> and C<sub>18</sub> using the sparger method [23]. On the other hand, it was shown that sucrose esters (SEs) with C<sub>16</sub> and C<sub>18</sub> chains in the presence of high sucrose concentration are very efficient to produce voluminous foams with very small bubbles ( $\approx 2\ \mu\text{m}$ ) when Kenwood mixer is utilized for foam generation [24,25]. The produced foams remain stable for more

\* Corresponding author at: Department of Chemical and Pharmaceutical Engineering, Faculty of Chemistry and Pharmacy, Sofia University, 1 James Bourchier Ave., 1164 Sofia, Bulgaria.

E-mail address: [sc@lcppe.uni-sofia.bg](mailto:sc@lcppe.uni-sofia.bg) (S. Tcholakova).

<https://doi.org/10.1016/j.molliq.2024.126491>

Received 26 August 2024; Received in revised form 7 November 2024; Accepted 11 November 2024

Available online 13 November 2024

0167-7322/© 2024 The Author(s). Published by Elsevier B.V. This is an open access article under the CC BY-NC license (<http://creativecommons.org/licenses/by-nc/4.0/>).

than a year at 4 °C [25]. Therefore, depending on the method used for foam generation, a different conclusion is drawn with respect to foamability of long-chain SEs. One of the aims of the current study is to analyze in detail what could be the reason for these differences and under which conditions voluminous foams with small bubbles can be formed from SEs solutions.

Brijis are polyoxyethylene alkyl ethers of structure  $C_nEO_m$  with relatively broad distribution of EO-groups in their head group [26]. Their properties are widely studied in the literature and results in terms of surface, aggregation, film, and bulk properties are very well documented [24,26–39]. They are known to be mild foaming agents: their foamability depends on the number of EO groups [33,36], the alkyl chain length [33,37], and foam stability is usually quite poor [21,33,36,38,39]. It was shown the existence of a maximum in foamability with the number of EO-groups [33,36], and wide distributions exhibit similar foamability as narrow distributions, but enhanced stability [26]. The increase of surfactant chain length leads to significant decrease in the amount of formed foam in fast foaming method (Bartsch test), whereas the longer chain Brij 58 with 16C-atoms is the most weight efficient surfactant to produce the stable foam in slow foaming method (foam rise test) [40]. Decreasing the intensity of hitting in the modified Bartsch test utilized in Ref. [41] led to better foamability of this solution. However, those surfactants are very sensitive to temperature and usually the foam stability decreases with temperature [34] and they act as antifoam agents above their cloud point [35]. There are numerous applications in which the stabilization of foams at high temperature is necessary such as enhanced oil recovery [1–5], laundry washing [42], food preparation [43,44], and the better understanding the factors affecting the foam stabilization at high temperatures is important for choosing the appropriate surfactants for these applications. One of the aims of the current study is to compare the foam properties of sucrose esters and Brijis in the temperature range between 25 and 60 °C. This temperature range is important for laundry washing [42] and food production [43,44].

This work is a continuation of our previous study [21], dedicated to investigating the foaming properties of Brij L23 and sucrose ester L1695, and focused on their respective response to temperature and the role of H-bonds. It was shown that for L1695, the adsorption of diesters was beneficial for foam stability, whereas foamability was enhanced by the rapid adsorption of monoesters. In those two  $C_{12}$ -chain surfactants, all investigated solutions had Newtonian behavior. In the current study, two additional sucrose esters with  $C_{16}$  and  $C_{18}$  chains, namely P1675 and S1570, are investigated and compared to their homologous Brijis (Brij 58 and Brij S20), to assess the impact of alkyl chain length on the various physicochemical aspects of foam generation and foam stability. A particular interest is set on the effect of temperature-induced phase changes, and related rheological properties, in solutions of sucrose esters for their foaming properties.

The methods implemented in this work rely on the investigation of (i) the bulk rheological properties, (ii) surface properties at equilibrium and under dynamic conditions, and (iii) thin liquid film behavior. Those properties are the basis for rationalizing the foaming properties in three foaming methods, namely the planetary mixer or Kenwood Mixer (KM), the Bartsch Test (BT), and the foam-rise method (FRM). Foams are discussed in terms of volume of air entrapped, bubble size, and destabilization phenomena.

The main problems addressed in the current study are: (1) What is the reason for the formation of foams with very big bubbles from long-chain sucrose ester solutions in slow foaming method (foam rise method); (2) What is the impact of non-Newtonian behavior of sucrose ester solutions on their foamability. The main novelty of this work is the observation of cyclic dimple in the foam films formed from a non-volatile substance, due to different composition of adsorption layers formed in film interior and in meniscus region.

## 2. Materials and methods

### 2.1. Materials and procedure for solution preparation

Sucrose esters L1695, with predominantly 12C-atom in its tail (denoted as  $C_{12}SE$  in the text), and S1570 (denoted as  $C_{18}SE$  in the text) with predominantly 18C-atoms in its tail were obtained from Ryoto™, whereas P1675 (denoted as  $C_{16}SE$  in the text below) with predominantly 16C-atom in its tail was obtained from TCI (Tokyo Chemical Industry Co., Ltd., Japan). They contain a mixture of mono-, di-, and tri-esters of sucrose, and a mixture of alkyl chains [45]. The HLB values given by the producer are 16 for  $C_{12}SE$  and  $C_{16}SE$  and 15 for  $C_{18}SE$  [45]. However, these values have a different meaning compared to traditional HLB values according to the classic definition of Griffin ( $HLB = 20 \times \frac{M_{hydrophilic\ part}}{M_{total}}$ ) because they represent the monoester content in the compound  $HLB \approx 20 \times [\text{monoesters content, \%}]/100$  [46,47]. Their composition, determined by HPLC and GC analyses, is given in section 3.1 and based on this, the HLB values according to Griffin's definition are calculated and shown in Table 1 below.

Polyoxyethylene (23) lauryl ether (Brij L23) with 12C-atoms in its tail and averaged number of 23 EO-groups in its head (denoted as  $C_{12}EO_{23}$  in the text), Polyoxyethylene (20) cetyl ether (Brij 58 – denoted as  $C_{16}EO_{20}$  in the text) with 16C-atoms and averaged number of 20 EO-groups, and Polyoxyethylene (20) stearyl ether (Brij S20 – denoted as  $C_{18}EO_{20}$  in the text) with 18C-atoms and averaged number of 20 EO-groups were obtained from Sigma-Aldrich. The average molecular masses of 1198.0 g/mol for Brij L23, 1122 g/mol for Brij 58, 1151.56 g/mol for Brij S20 are used for determining their molar concentrations. The HLB values of studied Brijis according to their producer are 16.9 ( $C_{12}EO_{23}$ ); 16.0 ( $C_{16}EO_{20}$ ) and 15.0 ( $C_{18}EO_{20}$ ).

All chemicals were used as received without any further purification. All solutions were prepared using deionized water obtained by an Elix 3 system (Merck-Millipore Inc., USA).

$C_{12}SE$  and  $C_{12}EO_{23}$  surfactant solutions were prepared by stirring the surfactant/water mixture at 60 °C for 30 min using a magnetic stirrer. Other surfactant solutions were prepared by stirring the surfactant/water mixture at 75 °C for 30 min using a magnetic stirrer. All concentrations are given as weight percentages relative to the solution weight. All solutions were used within 48 h after preparation.

### 2.2. HPLC and GC procedures for analysis of sucrose esters chemical composition

The procedures used are described in detail in Ref. [21]. Briefly, the fatty acid chain lengths were analyzed by GC after sucrose ester hydrolysis, whereas the ratio between monoesters and diesters was determined using HPLC.

### 2.3. Viscosity measurements

The viscosity of the solutions was measured with a modular compact rheometer MCR-302e (Anton Paar, Austria), using cone and plate geometry with a diameter of 40 mm (cone angle 1°, truncation gap 78 μm). Measurements were performed at 25.0, 40.0, 50.0, and 60.0 °C, and samples were equilibrated for 3 min before each measurement. The rheological test in a steady shear regime was performed by varying the shear rate logarithmically and stepwise from 0.01 s<sup>-1</sup> to 500 s<sup>-1</sup>. The viscosity was monitored as a function of shear rate. For reproducibility, each measurement was repeated twice, and the average results are presented.

### 2.4. Surface tension measurements

The surface tensions were measured using a Krüss K100 tensiometer (Krüss GmbH, Hamburg, Germany). A Du Nouy ring was used for the construction of surface tension isotherms. The temperature was kept

**Table 1**

Chemical composition of sucrose esters determined by HPLC (monoesters/ di- and triesters ratio) and GC after hydrolysis (alkyl chains length).

Denoted in the text	Commercial name of the surfactant	Monoesters content	Di/triesters content	Fatty acid composition			Calculated HLB value according to Griffin's definition
				n-C12	n-C16	n-C18	
C <sub>12</sub> SE	L1695	87 %	13 %	> 99 %	0	0	12.6
C <sub>16</sub> SE	P1675	80 %	20 %	0	80 %	20 %	11.0
C <sub>18</sub> SE	S1570	69 %	31 %	0	32 %	68 %	10.3

within 0.2 °C during the experiment by thermostat (Julabo GmbH, Germany) and thermostatic pump CORIO CD-200F to circulate the thermostated water.

Dynamic surface tension was measured by the maximum bubble pressure method (MBPM) with a processor-controlled bubble pressure tensiometer Krüss BP2 (Krüss GmbH, Hamburg, Germany) at fixed temperatures of 25.0 °C, 40.0 °C, 50.0 °C and 60.0 °C which were kept by circulating water using a CORIO CD-200F thermostatic pump (Julabo GmbH, Germany) with an accuracy of 0.2 °C. Hydrophobized glass capillaries with a hydrophilic tip were used for all measurements, and their diameter was measured before each set of experiments.

### 2.5. Film properties

A capillary cell was used to observe the behavior of thin foam films [48]. The films were formed in a capillary with a radius  $R = 1.25$  mm by sucking out the solution through a side orifice, and were observed in reflected light using a Leica DM RXE optical microscope (Leica Microsystems, GmbH; Wetzlar, Germany) equipped with long-distance objective Nplan 20x/0.4, a CCD camera (Sony SSC-C370P), and a 5.1 M Video Biological Microscope Digital Camera 55FPS LCMOS. The typical radius of the foam films formed in this capillary was  $R_F \approx 0.15$  mm. The temperature was controlled by using a steel cell-holder with inner water circulation using a CORIO CD-200F thermostatic pump (Julabo GmbH, Germany). The top glass cover was heated to avoid forming condensation droplets. The solution temperature was monitored using a type K thermocouple probe and a UT325 thermometer (Uni-Trend Technology co. Ltd., China). From the intensity of the reflected light, the foam film thickness was determined [48]. The film thinning pattern and the stability of the foam films were studied in closed cell in which the capillary pressure was 40–70 Pa. Each film was observed for 10 min after its formation. At least three different films were observed for a given concentration at a given temperature. The temperature was controlled with an accuracy of 1 °C.

The film thickness,  $h$ , was determined from the obtained images, which were converted to gray scale, and using the following expression [48]:

$$h = \frac{L}{2\pi n} \times \left( \frac{\delta}{2} \pm \arcsin \left( \sqrt{\frac{I - I_{min}}{I_{max} - I_{min}}} \right) \right) \quad (1)$$

Where  $L$  is the wavelength of the incident light (for white light, the peak is around 565–580 nm),  $n$  is the film refractive index,  $\delta$  is the phase lag,  $I$  is the intensity of the reflected light from the film,  $I_{max}$  is the maximal intensity of the reflected light of white film,  $I_{min}$  is the minimal intensity of the reflected light after film breakage. Intensities are determined using the ImageJ software.

### 2.6. Foamability and foam stability

Foams were generated using three distinct methods: the Bartsch test (BT), the foam rise method (FRM), and the planetary mixer method, also known as Kenwood Mixer (KM).

#### 2.6.1. Bartsch test

A glass cylinder of 120 mL, filled with 10 mL surfactant solution,

was shaken using an automated Bartsch test for 100 cycles at shaking period of 1.23 s (frequency = 0.813 s<sup>-1</sup>). The method is described in details in Ref. [37]. It was shown in [37] that the characteristic time for bubble expansion in this method is 10 ms. This characteristic time was determined on the base of performed optical observations of the process of bubble generation by high speed video camera [37]. To control the temperature, a 3000 W blow heater regulated by PID thermocontroller and AC phase regulator, connected to an in-chamber type K thermocouple probe, was used. Experiments were conducted at  $T = 25, 40, 50$  and  $60 \pm 1$  °C. At least three different cylinders were used to determine the foamability under the given conditions.

#### 2.6.2. Foam rise method

Foam was generated by blowing the air through a 1 cm diameter filter paper with 8–12 μm pores into 20 mL of the surfactant solution, contained in a glass column. Dimensions of the column are 2.8 cm internal diameter and 20 cm total height. The air flow rate of  $0.38 \pm 0.02$  L/min was maintained for 15 s. Experiments were conducted at  $T = 25, 40, 50$  and  $60 \pm 1$  °C and temperature was controlled by immersing the glass column inside a thermoregulated water bath. Foam height was visually monitored every minute for 10 min after air sparging was stopped. Each experiment was repeated three times.

#### 2.6.3. Planetary mixer

A planetary mixer Kenwood Chef Premier KMC 560 (1000 W) such as described in Ref. [49] was used. 300 mL of the surfactant solution was placed in a transparent vessel with total volume of 3250 mL. The mixing tool was rotated with a speed of 2 rotations per second (rps), generating a maximum shear rate of 62 s<sup>-1</sup> in the vessel, as explained in Ref. [49]. The volume of the generated foam was monitored as a function of the shearing time. After the foam volume stopped increasing, shearing was continued for an additional 10 min. The experiment was stopped at a maximum duration of 60 min. This experiment was conducted at 25 °C using 0.1 wt% and 1 wt% surfactant solutions.

#### 2.6.4. Foam characteristics

To characterize the foamability in all three methods, the volume of entrapped air,  $V_A$ , was obtained by subtracting the solution volume from the total volume (solution + foam). The foam stability was evaluated after stopping the agitation in Bartsch test, after stopping the air supply in FRM, and after sampling foam from KM and introducing it in a 120 mL cylinder (2.8 cm internal diameter and 20 cm total height). The remaining volume of entrapped air was monitored by visual observation every 2 min for 10 min after stopping the agitation, or every 10 min for 60 min in longer monitoring experiments. Foam stability was characterized by the ratio between the remaining air in the foam at the end of destabilization monitoring (either 10 min or 1 h) and the initial amount of air entrapped during foam generation. In order to compare foaming methods with one another, the relative foam volume was obtained by comparison to that of a reference system, namely 50 mM SDS (sodium dodecyl sulfate).

For each foaming method, the bubble average size for foams formed at 25 °C and resulting of 1 wt% surfactant solution was determined using the procedure developed by Garrett *et al.* [50]: a video camera, equipped with a long-working distance magnifying lens, was focused on the foam

sample in contact with a glass prism, and used to capture images of the bubbles. The sample is illuminated using white LED lights placed on the other side of the prism, so as to accentuate contrast between bubbles and plateau regions. Images are analyzed using the ImageJ software, yielding the projected bubble area,  $A_{BP}$ . Bubble radius is calculated as  $R_{BP} = \sqrt{A_{BP}/\pi}$ , and the volume median radius  $R_V(50)$  is obtained from the volume frequency distribution. At least 1000 bubbles were analyzed for each sample. Lower and upper error bars correspond to  $R_V(16)$  and  $R_V(84)$ , respectively.

In the FRM, the bubble formation on the membrane was observed in 0.1 wt% solutions using a high-speed camera and a long-working distance magnifying lens.

### 3. Experimental results and discussion

Section 3.1 presents the chemical composition of the sucrose esters used in this study, determined by GC and HPLC analysis, along with the rheological properties of 0.1 wt% and 1 wt% aqueous solutions. In Section 3.2, the measured surface tension isotherms and the determined characteristics of the adsorption layers are presented. These results are then used in section 3.3 to calculate the dynamic adsorption based on the measured dynamic surface tensions. The behavior of foam films is described in section 3.4. Finally, Sections 3.5 and 3.6 summarize the results of the foaming experiments and their interpretation, including the air entrapment capacity (foamability), average bubble size, and foam stability.

#### 3.1. Bulk properties of 0.1 wt% and 1 wt% solutions

##### 3.1.1. Chemical composition of alkyl sucrose esters

The chemical composition of all three sucrose esters was analyzed by HPLC to determine the monoester-to-diester ratio, and through GC after hydrolysis to establish the fatty acid chain length ratio. Analyses revealed a monoester content of 87 %, 80 %, and 70 % for L1695, P1675, and S1570, respectively. While alkyl chains in L1695 are > 99 % dodecyl chains, P1675 and S1570 both contain a mixture of palmitic and stearic chains: 80 % palmitic in P1675, and 68 % stearic in S1570. The obtained results are summarized in Table 1 for all three sucrose esters, and are in good agreement with the information provided by the manufacturers [45,51]. The mean chain length was determined to be 12 for L1695, 16.4 for P1675 and 17.4 for S1570. The estimated average molecular masses assuming random distribution of fatty acid chains in monoesters and diesters are 548 g/mol for L1695, 635 g/mol for P1675 and 679 g/mol for S1570. Note that the molecular masses of sucrose esters are  $\approx$  2-times smaller than those of used Brijis due to smaller head group in SEs.

For calculation of HLB of SEs we again assume random distribution of fatty acid chains in monoesters and diesters. It is seen from data shown in Table 1 that HLB values for SEs are noticeably lower (between 10.3 and 12.6) compared to those given for Brijis (between 15 and 16.9).

##### 3.1.2. Viscosity of studied solutions

The measured shear stress vs. shear rate dependencies revealed Newtonian behavior for all 0.1 wt% surfactant solutions, across the temperature range from 25 °C to 60 °C. The viscosity decreases as the temperature increases, see Fig. S1. A slight deviation is observed only for the 0.1 wt% C<sub>18</sub>SE solution, for which the viscosity measured at 50 °C is higher than that at 60 °C. At 25 °C the viscosities of Brijis solutions are higher than those of SEs, as shown in Fig. 1A, whereas at 60 °C all solutions have very similar viscosities. The impact of the aggregates' presence on the viscosity can be assessed by calculating the relative viscosity, defined as the ratio between the viscosity of the surfactant solution and that of water. The relative viscosity follows the same tendency for all surfactants, increasing from 1.1 to 1.3 to 1.5–1.6 as  $T$  increases from 25 to 60 °C. This suggests that the presence of micelles has the least impact on viscosity at  $T = 25$  °C and the highest at 60 °C. An exception to this rule is for C<sub>18</sub>SE at 50 °C, where the relative viscosity reaches 1.7 due to the formation of elongated micelles near the melting point of surfactant's tails [52–54].

Ten-fold increase of surfactant concentration for Brijis solutions (from 0.1 wt% to 1 wt%) does not significantly affect their behavior. A similar small effect is observed for C<sub>12</sub>SE, see Fig. S1. However, the behavior of the 1 wt% C<sub>16</sub>SE and C<sub>18</sub>SE solutions differ significantly. These solutions exhibit Newtonian behavior at 25 °C and non-Newtonian behavior at 50 °C and 60 °C. At 40 °C, 1 wt% C<sub>16</sub>SE has non-Newtonian behavior, whereas 1 wt% C<sub>18</sub>SE remains Newtonian, see Fig. S2. Such peculiar behavior has already been reported in the literature for sucrose stearate [52,53] and was investigated in detail for C<sub>16</sub>SE in our recent study [54]. It was shown that the coexistence of mono- and di-esters in C<sub>16</sub>SE resulted in the formation of discrete monodisperse diester particles coexisting with a network of partially fused diester particles at low temperature [54]. As the temperature approaches the diesters' melting point, wormlike mixed micelles form, causing a viscosity peak, although some diester particles persist in the solution [54]. Further increase in temperature causes fluidization of the surfactant tails and the formation of branched micelles, while the excess diester molecules phase-separate into distinct droplets [54]. The lower viscosity observed in C<sub>18</sub>SE compared to C<sub>16</sub>SE in the current study is probably related to the lower concentration of monoesters in C<sub>18</sub>SE compared to C<sub>16</sub>SE (70 vs. 80 %), which can incorporate into the wormlike micelles near the melting point of the diesters. Note that the transition melting temperature is higher for

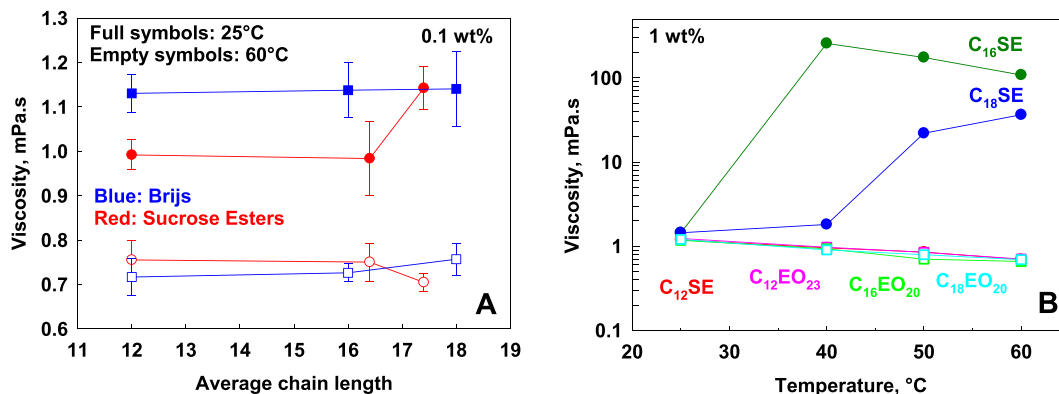


Fig. 1. (A) Viscosity as a function of the average chain length for Brijis (blue symbols) and alkyl sucrose esters (red symbols) in 0.1 wt% solutions measured at 25 °C (full symbols) and 60 °C (empty symbols); (B) Viscosity as a function of temperature for 1 wt% solutions of Brijis: C<sub>12</sub>EO<sub>23</sub>; C<sub>16</sub>EO<sub>20</sub> and C<sub>18</sub>EO<sub>20</sub> (empty symbols) and SEs: C<sub>12</sub>SE; C<sub>16</sub>SE and C<sub>18</sub>SE (full symbols) with varying chain lengths. For non-Newtonian fluids (C<sub>16</sub>SE and C<sub>18</sub>SE), the apparent viscosity at 1 s<sup>-1</sup> is shown, while for Newtonian fluids, the averaged viscosity determined from the slope of shear stress vs. shear rate is plotted. (For interpretation of the references to colour in this figure legend, the reader is referred to the web version of this article.)

sucrose stearate than that for sucrose palmitate (47 vs. 40 °C) [24], which explains why a higher temperature required to observe the viscosity increase in the former case.

### 3.2. Equilibrium surface properties

The surface tension isotherms for SEs ( $C_{16}SE$  and  $C_{18}SE$ ) and Brijs ( $C_{16}EO_{20}$  and  $C_{18}EO_{20}$ ) are presented in Fig. 2. For the surface tension isotherms of  $C_{12}SE$  and  $C_{12}EO_{23}$ , the reader is referred to Ref. [21]. As previously explained in the case of  $C_{12}SE$ , the presence of di- and triesters causes a continuous decrease in surface tension during measurements (not stabilized even after 1 h). This is due to the continuous substitution of adsorbed monoesters by diesters, which adsorb and desorb at a slower rate: on a short timescale, monoesters adsorb on the surface, but on a longer timescale, diesters gradually replace them. The same observation was made for  $C_{16}SE$  and  $C_{18}SE$  in the current study. Therefore, the diffusion-limited adsorption assumption is not verified, and the equilibrium surface tension cannot be determined from the intercept of  $\sigma$  vs.  $t^{-1/2}$  [37,40,55], see Fig. S3 of the SI. That is why, in the current study, surface tension isotherms are constructed using the surface tension measured after 10 min, which is close to the equilibrium surface tension that is expected to be reached in the presence of only monoester molecules. Over longer time scales, diester molecules continue to adsorb, further decreasing the surface tension. However, these diester molecules do not contribute to the properties of adsorption layers during the foam generation. While they significantly impact the stability of the foam, the current study focuses on the characteristics of the adsorption layers responsible for the foam generation, and all the characteristics of adsorbed layers given below refer to the detailed study

of the foam generation process.

A similar approach to use the surface tension measured at intermediate times for construction of surface tension isotherm, was proposed in the foundational work of Mysels for determining the surface tension of sodium dodecyl sulfate solutions in the presence of dodecanol impurities [56]. It was shown that thermodynamically meaningful equilibrium surface tension values are obtained at intermediate times: after the adsorption of the primary surfactant component is nearly complete and before significant adsorption of highly surface-active impurities begins [56,57]. In our study, we aim to determine the adsorption of sucrose monoesters, which are at higher bulk concentrations than sucrose diesters in the solution, although they are less surface active. For this reason, we use the surface tension measured after 10 min, where the monoester adsorption is complete but diester adsorption has not yet started as discussed above. At this stage, the monoester molecules within the adsorption layer are in equilibrium with those in the bulk, allowing us to apply the Gibbs adsorption isotherm.

The determined isotherms are analyzed to extract the key characteristics of the studied surfactants: (1) critical micellar concentration, CMC; (2) surface tension at CMC,  $\sigma_{CMC}$ ; (3) surfactant adsorption at CMC,  $\Gamma_{CMC}$ ; (4) excluded area per molecule,  $\alpha$ , which is used for determining instantaneous adsorption from the measured dynamic surface tension in the next section, and (5) surface pressure at CMC,  $\pi_{CMC}$ , defined as the difference between the surface tension of pure water at a given temperature and the surface tension measured in the presence of a surfactant at a concentration equal to the CMC at the same temperature.

The surface tension data below the CMC were used to calculate the surfactant adsorption at CMC,  $\Gamma_{CMC}$  ( $\mu\text{mol}/\text{m}^2$ ), by using Gibbs' equation [55]:

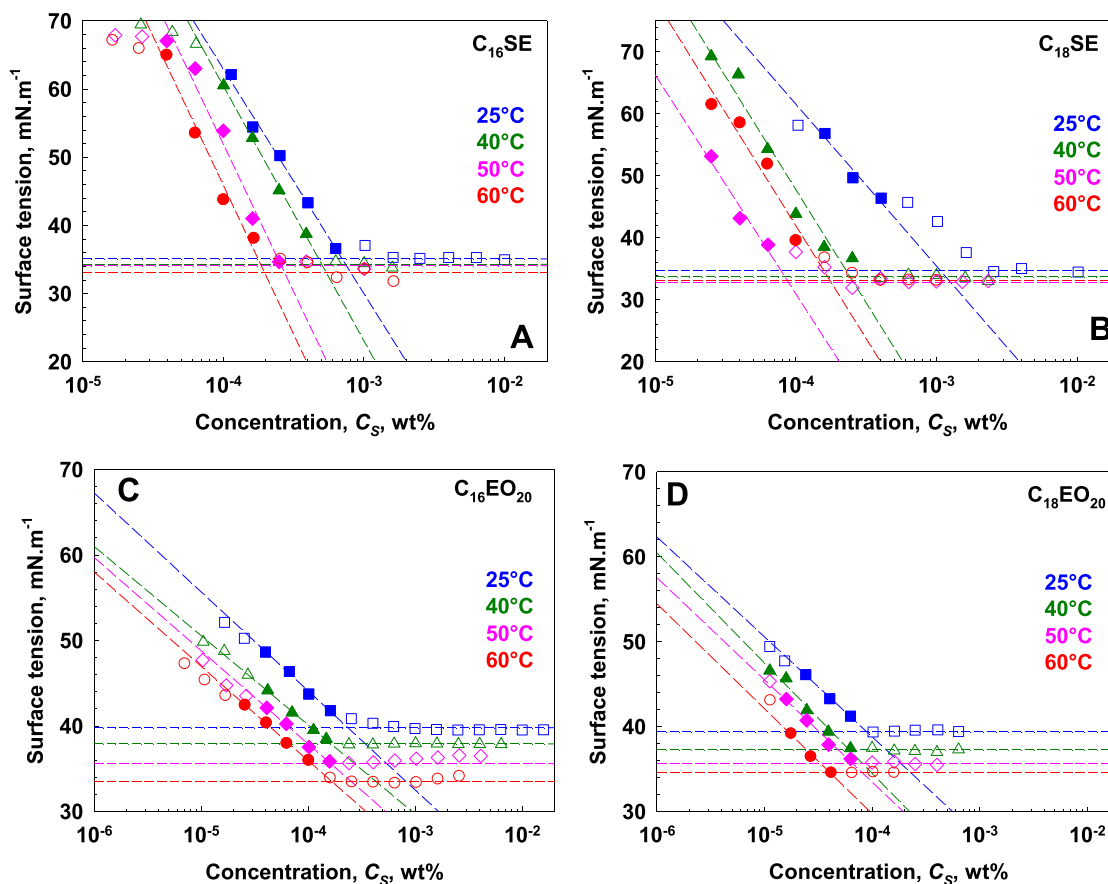


Fig. 2. Surface tension isotherms for SEs: (A)  $C_{16}SE$  and (B)  $C_{18}SE$ , and for Brijs: (C)  $C_{16}EO_{20}$  and (D)  $C_{18}EO_{20}$ , measured at temperatures,  $T$ , ranging from 25.0 °C to 60.0 °C. Surface tension values,  $\sigma$ , are taken after 10 min using the du Nouy ring method. Before the plateau region, the points used for the regression are shown in full symbols.

$$\frac{d\sigma}{d\ln C_s} = -RT\Gamma_{\text{CMC}} \quad (2)$$

In this equation,  $\Gamma_{\text{CMC}}$  is the surfactant adsorption at CMC,  $\sigma$  is the measured surface tension after 10 min,  $R$  is the gas constant,  $T$  is the temperature, and  $C_s$  is the bulk surfactant concentration.

As explained in our previous studies [21,38,41], the excluded area per molecule  $\alpha$  can be calculated from the determined surfactant adsorption at CMC using the Gibbs adsorption isotherm and the measured surface pressure at CMC, assuming that adsorption can be described by Volmer's equation [37]. The value of excluded area per molecule,  $\alpha$ , is used afterwards to determine the instantaneous adsorption from the measured dynamic surface pressure. For further details, see explanations given in Ref. [37].

$$\alpha = \frac{\pi_{\text{CMC}} - RT\Gamma_{\text{CMC}}}{\pi_{\text{CMC}}\Gamma_{\text{CMC}}N_A} \quad (3)$$

where  $N_A$  is the Avogadro number, and  $\pi_{\text{CMC}}$  is the surface pressure defined as  $\pi_{\text{CMC}} = \sigma_0 - \sigma_{\text{CMC}}$ , with  $\sigma_0$  being the surface tension of pure water, taken to be 72.0, 69.6, 67.9, or 66.2  $\text{mN}\cdot\text{m}^{-1}$  at 25 °C, 40 °C, 50 °C or 60 °C, respectively. Before the plateau region, a well-defined region, in which the surface tension decreases linearly with  $\ln C_s$ , is used to determine  $\Gamma_{\text{CMC}}$  using eq. (2). The cross point between the linear dependence of  $\sigma$  vs.  $\ln C_s$  and the minimal surface tension measured under the given conditions is used to calculate the CMC. The extracted characteristics as a function of temperature are shown in Fig. S4 of the SI, and their evolution with the alkyl chain length is presented in Fig. 3.

For similar chain lengths, and regardless of the temperature, all three sucrose esters exhibit higher CMC than Brijs. This indicates a higher molecular solubility in the aqueous phase for sucrose esters, attributed to the sucrose polar head higher solubility, since the alkyl chain solubility for homologous molecules is expected to be lower for SEs due to

the presence of diesters. Note that there is no direct correlation between CMC and HLB values, as HLB values for SEs are lower than those of Brijs while their CMC is higher. Therefore, HLB values cannot explain the higher CMC for SEs.

For most of the surfactants investigated, the CMC value decreases with  $T$ , which is a non-trivial behavior. The typical behavior reported for both ionic and nonionic surfactants is a U-shaped evolution of CMC with  $T$  [30,58–61]. Only  $C_{18}\text{SE}$  exhibits this type of behavior, the lowest CMC value being reached at 50 °C, see Fig. S4. The non-detection of a minimal CMC value over the  $T$  range for the other five surfactants can be due to a lack of data at higher temperature. On the decreasing part of the CMC vs.  $T$  curve, the hydrogen bonds between water and the surfactant polar head get weakened and molecules appear more hydrophobic. At the same time, increasing  $T$  also contributes to increasing the aqueous solubility of the alkyl chains. Once the CMC passes through its minimum, the increased solubility effect counterbalances, and then overcomes, the polar head dehydration effect. Both effects respectively prevent and facilitate the micellization [60].

The chain length effect within each group – Brijs on one side, and SEs on the other – differs significantly. Typically, the CMC decreases by 1 order of magnitude when increasing the alkyl chain length by 2 carbon atoms for nonionic surfactants and by 3-carbon atoms for ionic surfactants. This phenomenon is due to the increased hydrophobicity of the alkyl chain [61–64]. This trend is verified for Brijs, but not for SEs as CMC values for  $C_{16}\text{SE}$  and  $C_{18}\text{SE}$  are in the same order of magnitude at 25 °C, and very similar to those reported in [22]. The most probable reason for this behavior is the presence of both diester and monoester molecules with  $C_{16}$  and  $C_{18}$  chains in varying ratios in these surfactants, resulting in a similar number of free molecules for both surfactants. More hydrophobic compounds (sucrose diesters) trigger the formation of solid particles, as shown for  $C_{16}\text{SE}$  [54].

It was previously shown that increasing  $T$  from 25 °C to 60 °C has

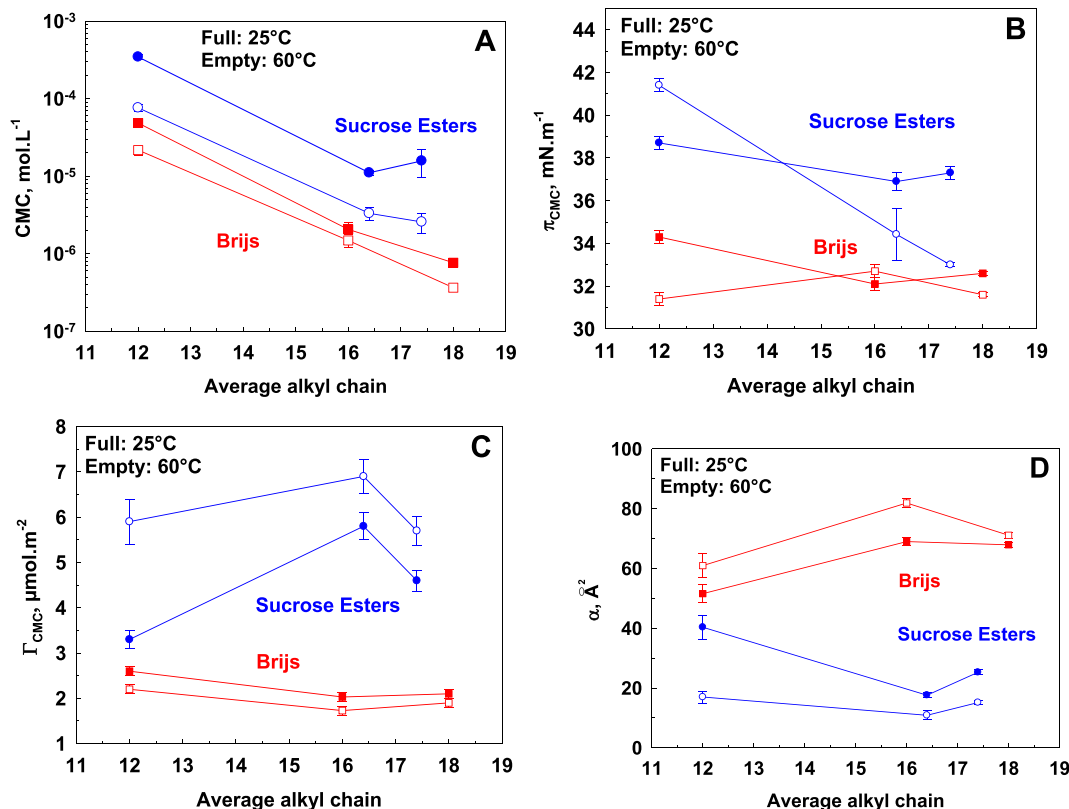


Fig. 3. Surface characteristics at CMC as a function of alkyl chain length: (A) CMC obtained as the intersection of the plateau region and the linear decrease in surface tension with concentration, (B) surface pressure at CMC,  $\pi_{\text{CMC}}$ , (C) surface concentration,  $\Gamma_{\text{CMC}}$ , obtained by equation (2), and (D) excluded area per molecule,  $\alpha$ , calculated at CMC using equation (3). Data for  $C_{12}\text{SE}$  and  $C_{12}\text{EO}_{23}$  are taken from Ref. [21].

opposite effect on  $C_{12}SE$  and  $C_{12}EO_{23}$  adsorption at CMC,  $\Gamma_{CMC}$ : while it increases for  $C_{12}SE$ , it decreases for  $C_{12}EO_{23}$ . For  $C_{12}SE$ , this was attributed to the higher adsorption of diesters and the formation of denser layers at elevated temperature [21]. In accordance with this explanation, a similar behavior is observed for  $C_{16}SE$  and  $C_{18}SE$ , which also contains diester molecules. Accordingly, the excluded area per molecule,  $\alpha$ , slightly decreases with  $T$  for both  $C_{16}SE$  and  $C_{18}SE$  as it was the case for  $C_{12}SE$ . In sucrose esters, the increase in alkyl chain entropy with  $T$  is overcome by the additional adsorption of diesters, contributing to the decrease in the area per molecule. Note that in  $C_{16}SE$ , the  $\alpha$  value reaches a small value of approximately  $11 \text{ \AA}^2$ , indicating the formation of condensed layers at the air–water interface. However, this is smaller than the cross-section area of frozen surfactant tails [65]. This discrepancy can arise from our assumption that isotherms could be described by Volmer's equation, as  $C_{16}SE$  and  $C_{18}SE$  present a substantial number of non-soluble particles, and not only solubilized molecules. In that case, Volmer's equation does not fully apply since the equilibrium with the surface is not the only one to be considered, given the presence of particles. Among Brijis, the evolution of  $\Gamma_{CMC}$  with  $T$  for  $C_{16}EO_{20}$  and  $C_{18}EO_{20}$  follows the same tendency as that of  $C_{12}EO_{23}$ , showing a slight decrease. This is in line with the evolution of the excluded area per molecule,  $\alpha$ , as it slightly increases over  $T$ : as each molecule occupies more surface, the adsorption is reduced. The experimental data obtained with Brijis, showing a slight decrease in  $\Gamma_{CMC}$  with temperature, aligns well with results reported in the literature for  $C_{12}EO_{20}$  [21,66],  $C_{18}EO_{10}$  [67],  $C_{18}EO_{20}$  [68], and pure  $C_8EO_8$  [57]. Notably, this slight decrease in adsorption with temperature is also observed for Tween 20, Tween 60, Tween 80, and their mixtures [68], as well as for the cationic surfactant CTAB [69]. In contrast, sucrose esters display an unusual behavior, with increased adsorption at higher temperatures which is probably related to higher adsorption of diester molecules at higher temperature.

The surface pressure at the CMC,  $\pi_{CMC}$ , plotted in Fig. 3B, evolves differently among sucrose esters: while it increases with temperature for  $C_{12}SE$ , it decreases for longer alkyl chain sucrose esters. This is due to the fact that the surface of  $C_{12}SE$  undergoes more changes from  $25 \text{ }^\circ\text{C}$  to  $60 \text{ }^\circ\text{C}$  compared to those of  $C_{16}SE$  and  $C_{18}SE$ . At  $25 \text{ }^\circ\text{C}$ , the adsorption of diesters is not observed in  $C_{12}SE$ , while it is in  $C_{16}SE$  and  $C_{18}SE$ , and  $C_{12}SE$  diesters adsorb on the surface at higher  $T$ . This greater surface evolution is also visible in terms of  $\Gamma_{CMC}$  and  $\alpha$ , with the surface of  $C_{12}SE$  being almost twice as dense at  $60 \text{ }^\circ\text{C}$ , compared to  $25 \text{ }^\circ\text{C}$ . The decrease of  $\pi_{CMC}$  with  $T$  in  $C_{16}SE$  and  $C_{18}SE$  indicates that the  $T$ -induced layer densification does not overcome the decrease in water surface tension (from  $72.0$  down to  $66.2 \text{ mN}\cdot\text{m}^{-1}$ ).

### 3.3. Dynamic properties of adsorption layers

Previous studies showed that foaming processes occur on a very short timescale, and equilibrium is not necessarily reached under these conditions [37,40]. Instead, it makes more sense to discuss the dynamic surface tension at the characteristic adsorption time for the foaming method. The previously developed method accounts for the foamability in FRM, KM, and BT, based on their respective surfactant adsorption characteristic times, which were found to be of  $10 \text{ ms}$  for BT,  $400 \text{ ms}$  for KM as measured in MBPM and  $50 \text{ s}$  as measured in Wilhelmy plate method for FRM [40]. This was verified in the case of  $C_{12}EO_{23}$  and  $C_{12}SE$  in the BT and FRM methods, for  $T$  ranging from  $25 \text{ }^\circ\text{C}$  to  $60 \text{ }^\circ\text{C}$ , and at  $25 \text{ }^\circ\text{C}$  in  $6 \text{ M}$  urea solutions [21]. In the same approach, the dynamic surface pressure,  $\pi_s(t)$ , was measured by the maximum bubble pressure method for three surfactant concentrations ( $0.01 \text{ wt}\%$ ;  $0.1 \text{ wt}\%$  and  $1 \text{ wt}\%$ ), and for  $T$  ranging from  $25 \text{ }^\circ\text{C}$  to  $60 \text{ }^\circ\text{C}$ . Experimental curves are presented in Fig. 4 and Fig. S5.

It appears that  $T$  impacts the kinetics of adsorption by making it faster, as all  $\pi_s(t)$  curves are left-shifted when increasing  $T$  from  $25 \text{ }^\circ\text{C}$  to  $60 \text{ }^\circ\text{C}$ . Increasing the bulk concentration also accelerates the adsorption kinetics for all 6 surfactants. For some solutions, there exists a plateau region for which  $\pi_s \approx 0 \text{ mN}\cdot\text{m}^{-1}$  before it increases, even though this region shortens with  $C_s$  and  $T$ . The length of this plateau region was evaluated as the time required to reach  $\pi_s = 2 \text{ mN}\cdot\text{m}^{-1}$ , see Fig. 5.

The time required to see an increase in  $\pi_s$  is the longest for sucrose esters  $C_{16}SE$  and  $C_{18}SE$ , even for a bulk concentration  $C_s = 1 \text{ wt}\%$ . The presence of lag time is well established in the literature for proteins [70] and polymers [71]. It was shown that the lag time for bovine serum albumin decreases with protein concentration [72,73], in agreement with the observed decrease for  $C_{16}SE$  and  $C_{18}SE$  in the current study. This phenomenon was already reported in Ref. [74] for  $0.1 \text{ wt}\%$  solution of sucrose stearate SP 70, with an induction period of  $t_{age} \approx 6.2 \text{ s}$ , very close the one observed for  $C_{18}SE$  ( $t_{age} \approx 7.1 \text{ s}$ ) in the current study. The smaller molecular weight of  $C_{16}$  and  $C_{18}$  sucrose esters compared to that of homologous Brijis seems to be in contradiction with their slower diffusion rate. It is also counter-intuitive given that CMC values for sucrose esters are higher than those of Brijis, indicating higher molecular solubility, that would lead to higher bulk availability. A main difference of SEs with Brijis also lies in the distribution of EO groups for Brijis: for an average number of 20 EO groups, Brijis also contain much smaller molecules with faster diffusion rates. This results in step-wise adsorption [71], as shorter molecules diffuse and adsorb faster on the surface.

The  $\pi_s(t)$  results were used to calculate the dynamic adsorption as a function of universal surface age,  $t_u$ , for Brijis. It is calculated by dividing

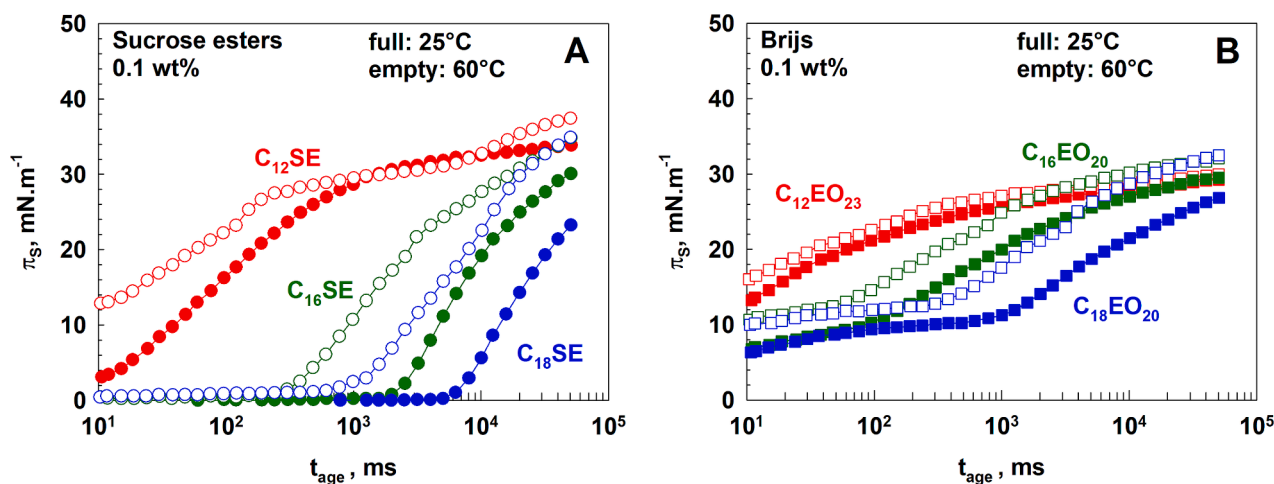


Fig. 4. Surface pressure evolution,  $\pi_s$ , over surface age,  $t_{age}$ , for  $0.1 \text{ wt}\%$  surfactant solutions: sucrose esters (A) and Brijis (B). Experiments are conducted at  $25 \text{ }^\circ\text{C}$ ,  $40 \text{ }^\circ\text{C}$ ,  $50 \text{ }^\circ\text{C}$ , and  $60 \text{ }^\circ\text{C}$ . For clarity, only the curves at  $25 \text{ }^\circ\text{C}$  and  $60 \text{ }^\circ\text{C}$  are represented, as the curves corresponding to experiments at  $40 \text{ }^\circ\text{C}$  and  $50 \text{ }^\circ\text{C}$  are positioned in between.

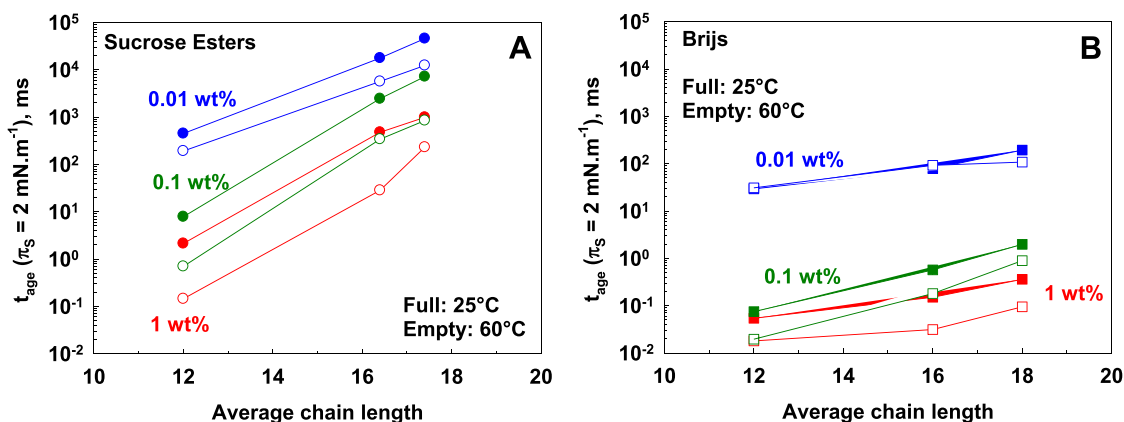


Fig. 5. Nominal surface age required to reach a surface pressure of  $2 \text{ mN}\cdot\text{m}^{-1}$ ,  $t_{age}(\pi_s = 2 \text{ mN}\cdot\text{m}^{-1})$ , at  $25^\circ\text{C}$  (full symbols) and  $60^\circ\text{C}$  (empty symbols), as a function of alkyl chain length for 1 wt%, 0.1 wt%, and 0.01 wt% solutions of (A) sucrose esters and (B) Brij surfactants. Results are obtained using the maximum bubble pressure method. Note that  $t_{age}$  values inferior to 10 ms are extrapolated.

the nominal surface age as provided by the apparatus,  $t_{age}$ , by 37 [75]. The dynamic adsorption,  $\Gamma(t)$ , and the dynamic surface coverage,  $\theta(t)$ , are calculated using the following expressions [37]:

$$\Gamma(t) = \frac{1}{\alpha N_A} \times \frac{\frac{\pi_s(t)\alpha N_A}{RT}}{1 + \frac{\pi_s(t)\alpha N_A}{RT}} \quad (4)$$

$$\theta(t) = \frac{\Gamma(t)}{\Gamma_{CMC}} \quad (5)$$

where the dynamic surface pressure,  $\pi_s(t)$ , is related to the measured dynamic surface tension by  $\pi_s(t) = \sigma_0 - \sigma(t)$ . Note that for determining the dynamic adsorption, the value of the excluded area per molecule,  $\alpha$ , must be known. It is determined from the adsorption isotherms presented in section 3.2 above. It should be mentioned that this approach is somewhat questionable for long chain sucrose esters  $C_{16}\text{SE}$  and  $C_{18}\text{SE}$  because of the presence of particles, making Volmer's equation inapplicable directly, but in first approximation under the assumption that there is an equilibrium between the monomers, micelles and particles, this approach can be applied. The obtained results are shown in Fig. 6.

The dynamic adsorption  $\Gamma(t_u = 10 \text{ ms})$  decreases with surfactant chain length for both SEs and Brij surfactants, see Fig. 6C and D at the three studied concentrations. The decrease is much more pronounced for SEs than for Brij surfactants. On the other hand, the dynamic surface coverage remains almost constant for Brij surfactants at  $C_s \geq 0.1 \text{ wt}\%$ , because the equilibrium surfactant adsorption  $\Gamma_{CMC}$  values for  $C_{12}\text{EO}_{23}$  is higher compared to those of  $C_{16}\text{EO}_{20}$  and  $C_{18}\text{EO}_{20}$ , and  $\theta$  values for all 3 Brij surfactants are comprised in the 70–100 % interval.

Regarding sucrose esters,  $C_{12}\text{SE}$  shows high  $\pi_s(t_u = 10 \text{ ms})$  values above  $25 \text{ mN}\cdot\text{m}^{-1}$  except at the lowest concentration, while longer chain sucrose esters remain with much lower  $\pi_s(t_u = 10 \text{ ms})$  values. Only  $C_{16}\text{SE}$  at the highest concentration and the highest  $T$  reaches a value of  $20 \text{ mN}\cdot\text{m}^{-1}$ . This is mostly due to  $C_{16}\text{SE}$  and  $C_{18}\text{SE}$  slow kinetics of adsorption,  $t_u = 10 \text{ ms}$  being a short timescale. In accordance with the tendency observed in Fig. 4, the temperature tends to increase  $\pi_s(t_u = 10 \text{ ms})$  for  $C_{16}\text{SE}$  and  $C_{18}\text{SE}$  as both of them have the steepest  $\pi_s(t)$  increase after the first plateau region. However, for both surfactants and for  $C_s = 0.01 \text{ wt}\%$ , the plateau region is longer than  $t_u = 10 \text{ ms}$  regardless of  $T$ , and  $\pi_s(t_u = 10 \text{ ms})$  remains  $\approx 0$ . The chain length influence on the dynamic characteristic of the surface differs significantly between each group of surfactants: while differences in terms of  $\pi_s(t_u = 10 \text{ ms})$  are tremendous amongst SEs, they are of lesser importance amongst Brij surfactants.

### 3.4. Thin film properties

The behavior of foam films was investigated for 0.1 wt% solutions of all 6 surfactants. In all cases, the observed film thinning behavior was typical for low molecular mass surfactants films, without the formation of condensed adsorption layer, and without film rupture within 10 min. The equilibrium film thickness was reached  $\approx 1 \text{ min}$  after film formation, during which a fast ejection of the entrapped dimples had occurred. Note that in presence of condensed adsorption layer on the film surfaces, the rate of dimple ejection would be over 10 min [75]. Illustrative images from these experiments are shown in Fig. 7.

Overall, thinner films are formed in Brij surfactants compared to SEs, with the formation of thin black films of about 30 nm. The values of measured film thickness,  $h$ , are given in Table S1, and the evolution with chain length in each surfactant group is shown in Fig. 8A. Black films appear only for  $T = 60^\circ\text{C}$  in  $C_{12}\text{EO}_{23}$ , but appear for  $T \geq 40^\circ\text{C}$  in  $C_{16}\text{EO}_{20}$  and  $C_{18}\text{EO}_{20}$ . They remain stable over the whole experiment duration, i.e., 10 min. In our previous study, films formed with 1 wt% solution of  $C_{12}\text{EO}_{23}$  showed this behavior for  $T \geq 25^\circ\text{C}$  [21]. The difference observed between both concentrations was attributed to a decrease in repulsion upon increasing  $C_s$ , displacing  $\text{HO}^-$  ions from the interface [21].

Thicker films are obtained with SEs, with no significant evolution over  $T$  for  $C_{12}\text{SE}$  and  $C_{16}\text{SE}$ . Literature data showed that  $\text{HO}^-$  adsorbs on the sugar-type polar heads, resulting in strong electrostatic repulsion in thin films, and this was shown to be the case for  $C_{12}\text{SE}$  in our previous work [21] and in [76] for alkyl polyglucosides. Here, the same phenomenon is seen for  $C_{16}\text{SE}$  and  $C_{18}\text{SE}$ . Those electrostatic charges are screened when forming sucrose ester thin films in 10 mM NaCl solutions, resulting in thinner and darker films, see Fig. S6. Note that the measured conductivity of the SEs and Brij solutions is similar and very low, as shown in Table S1. Therefore, the electrostatic repulsion does not stem from anionic species in these compounds but rather from the adsorption of hydroxyl ions. According to the literature, films formed from alkyl polyglucosides, even at a concentration of 0.45 mM, exhibit a thickness greater than 100 nm (see Ref. [76]). In the current study, the SE concentration is 1.5 mM and is still insufficient to remove all hydroxyl ions from the interface, the films thus remaining thick.

The behavior of  $C_{18}\text{SE}$  films differ from those of  $C_{12}\text{SE}$  and  $C_{16}\text{SE}$  as the film thickness increases for  $T \geq 40^\circ\text{C}$ , and dimples of  $h \approx 275 \text{ nm}$  are formed at  $T = 50^\circ\text{C}$ . Those dimples are different from initially non-ejected hydrodynamic dimples as they form and grow out of the thin film area, and indicate that water is being sucked from the film peripheric area. Such dimples were previously observed in emulsion films, and were attributed to surfactant diffusion from the aqueous film to the oil phase, leading to local depletion and Marangoni effect [77]. In

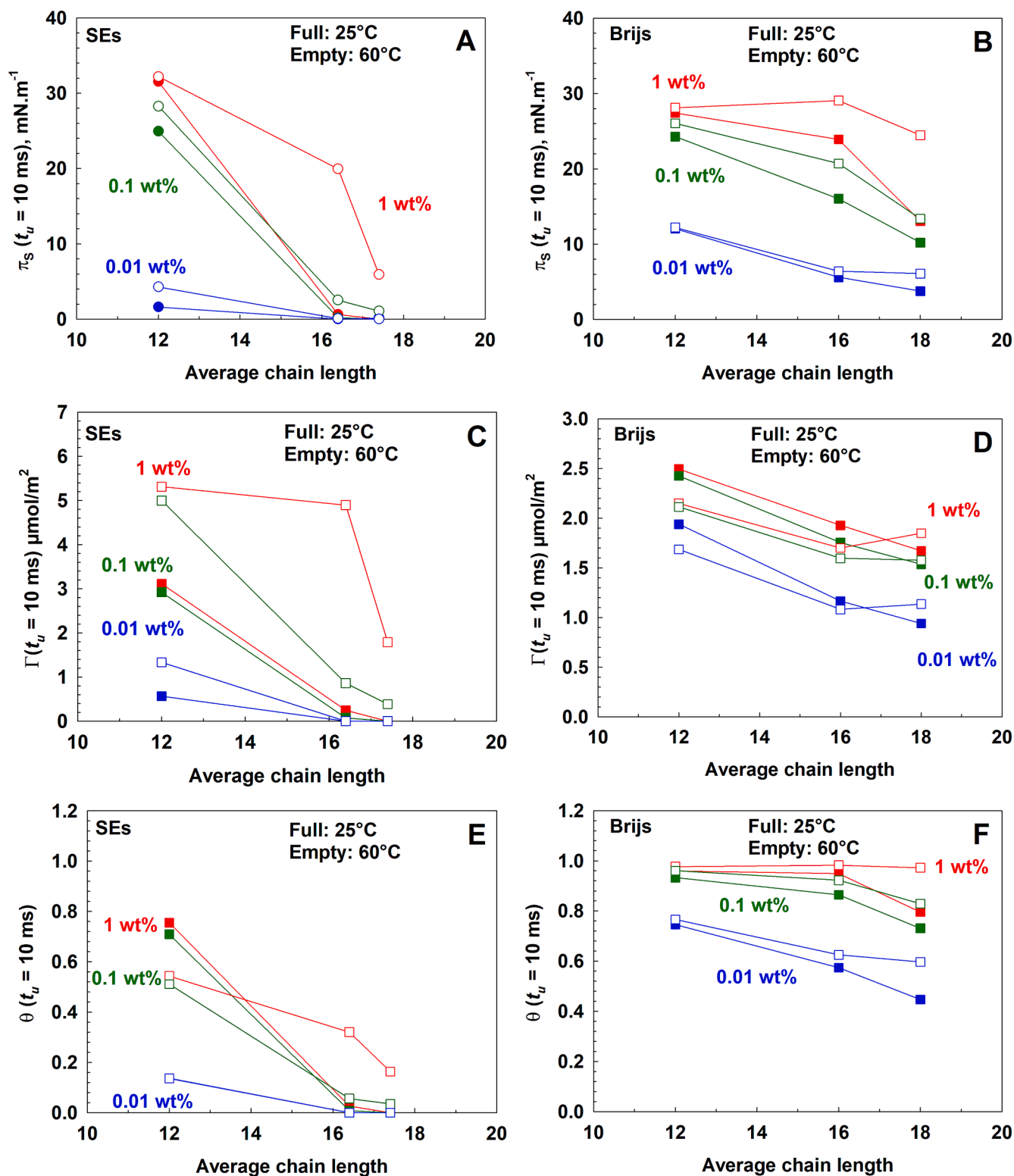


Fig. 6. (A, B) Dynamic surface pressure,  $\pi_s$ , (C, D) dynamic surfactant adsorption,  $\Gamma$ , and (E, F) dynamic surface coverage,  $\theta$ , determined after 10 ms universal surface age ( $t_u = 10$  ms) as a function of average chain length for sucrose esters (A, C, E) and Brij solutions (B, D, F) at 25 °C (full symbols) and 60 °C (empty symbols).

silicone oil thin films, this effect was attributed to the evaporation of volatile compound, leading to local concentration and surface tension increase, and triggering Marangoni effect [78]. In our case, the vessel being closed, no evaporation process is involved. The observed phenomenon in our case is most probably related to the Marangoni effect triggered by uneven distribution of diester molecules within the film and

meniscus region. The diester molecules are mainly incorporated in particles that just start to melt at 50 °C. However, during the film formation, those particles are expelled from the film and go to the meniscus. During film thinning, those particles provide the diester molecules which are able to adsorb on the meniscus region and are able to decrease the surface tension there, whereas the surface tension on film

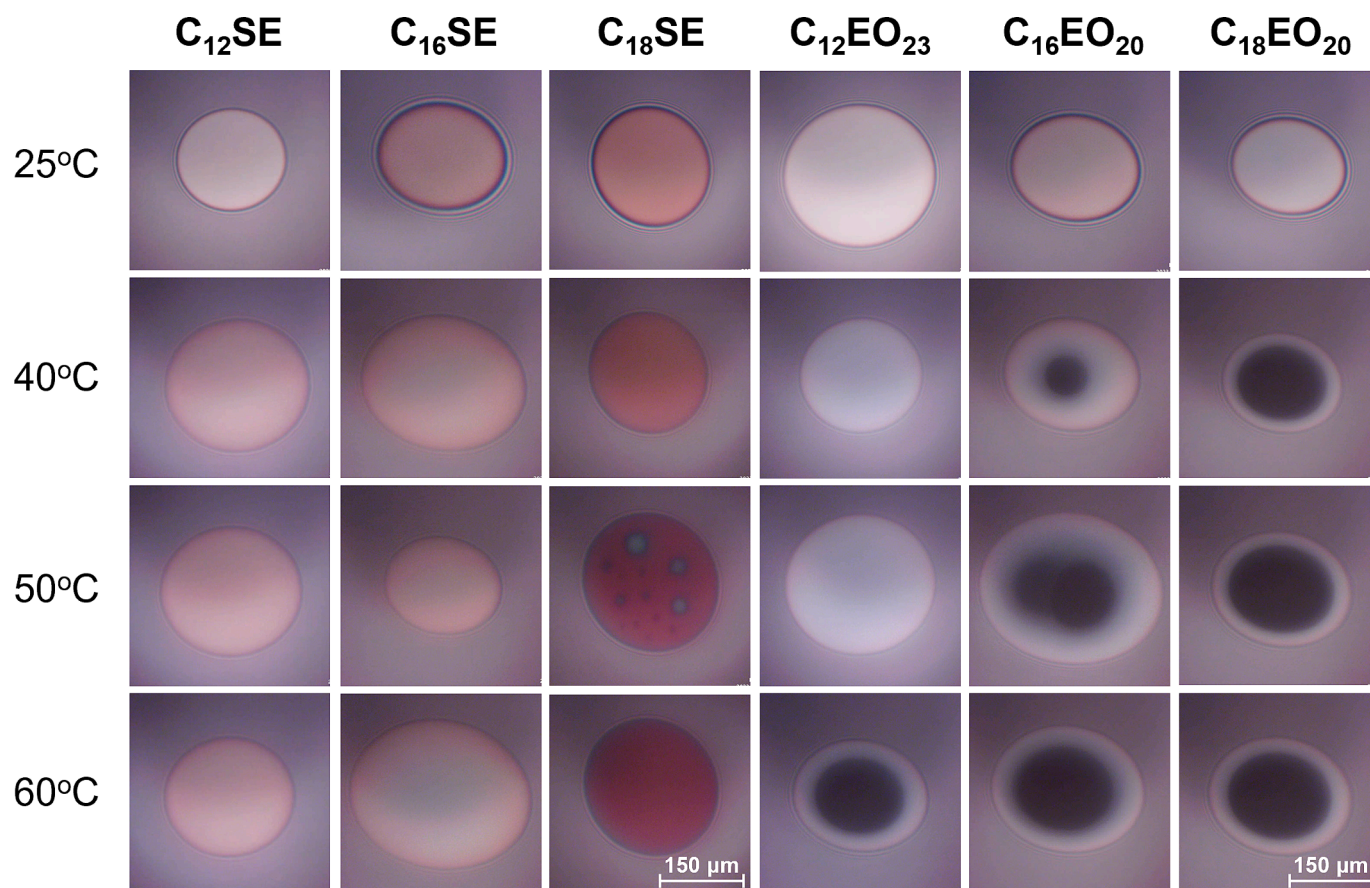


Fig. 7. Thin liquid films formed from 0.1 wt% solutions of SEs (left) and Brijis (right) solutions, observed under polychromatic white light using an optical microscope at 25 °C, 40 °C, 50 °C, and 60 °C. Pictures are taken 10 min after the film is created.

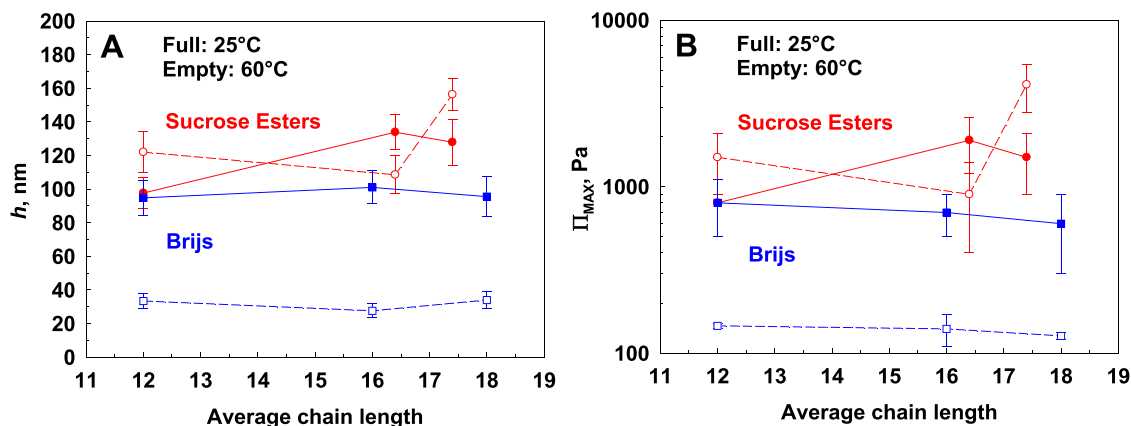


Fig. 8. (A) Film thickness,  $h$ , and (B) disjoining pressure,  $\Pi_{MAX}$ , evolution with average chain length for Brijis and sucrose esters at 25 °C (full symbols) and 60 °C (empty symbols) for films formed from 0.1 wt% surfactant solutions.

surfaces remain higher due to adsorption of monoester mainly. As a consequence, the Marangoni effect starts and drags water molecules from the meniscus to the film region.

To assess the strength of electrostatic repulsion and its effect on the film behavior, the magnitudes of the electrostatic and van der Waals interactions were estimated using [55]:

$$\Pi = 64n_0k_B T \left( \tanh \frac{e\Psi_S}{4k_B T} \right)^2 \exp(-\kappa h) - \frac{A_H}{6\pi h^3} \quad (6)$$

where  $\Pi$  is the disjoining pressure acting between film surface,  $n_0$  is the

electrolyte number concentration,  $k_B T$  is the thermal energy,  $\kappa$  is the inverse Debye screening length,  $\Psi_S$  is the electrical surface potential,  $e$  is the elementary charge,  $A_H$  is the Hamaker constant, and  $h$  is the film thickness. The Hamaker constant varies between  $3.73 \times 10^{-20}$  J at 25 °C and  $3.76 \times 10^{-20}$  J at 60 °C for all solutions, calculated using a dielectric constant of 78.3, 73.2, 69.9, and 66.8 for water at 25 °C, 40 °C, 50 °C, and 60 °C respectively [79] and a refractive index of 1.333 (negligible variations over the  $T$  range [80]). The solutions' conductivities were measured and used to estimate the ionic strength of the background electrolyte, considered to be NaCl (see Table S1). The characteristic Debye length,  $\kappa^{-1}$ , was then calculated using the previously stated

dielectric constant values, and varies between 26.1 nm ( $C_{12}EO_{23}$  at 60 °C) and 30.3 nm ( $C_{16}EO_{20}$  at 25 °C). The detailed information for the performed calculations is available in our previous paper [21] where the same approach is used for  $C_{12}EO_{23}$  and  $C_{12}SE$ . It should be mentioned that at such low electrolyte concentration, the electrolyte concentration in the film and in the meniscus region can differ due to ion confinement effects [81].

The capillary pressures,  $P_C$ , leading to film thinning were calculated using the measured equilibrium surface tensions, and varied between 40 Pa and 67 Pa, see Table S1. The stability of thin films is a balance between the capillary pressure on one side, attracting each surface towards the other, and the disjoining pressure on the other side, expressing the repulsive forces between surfaces. Different tendencies are observed between Brijis and SEs: while SEs maintain relatively high surface potential values with  $|\Psi_s|$  ranging from 36 to 122 mV, films formed with Brijis have much lower  $|\Psi_s|$  values, decreasing from about 35 mV at 25 °C down to 15 mV at 60 °C, see Table S1. This leads to much higher  $\Pi_{MAX}$  in SEs, which contributes to preventing rupture.  $\Pi_{MAX}$  dependence on chain length for both series of surfactants is shown in Figure 8B. The stability of all investigated films can be accounted for by the maximum disjoining pressure values:  $\Pi_{MAX}$  remains higher than  $P_C$ , meaning that electrostatic repulsion is sufficient to prevent a transition from electrostatically stabilized films to sterically stabilized ones, and eventually film rupture. In Brijis,  $\Pi_{MAX}$  values are lower than in SEs and dramatically decreases with  $T$ , in accordance with  $h$  decrease, but remain high enough to counterbalance the capillary pressure. In both series, the evolution of  $\Pi_{MAX}$  with chain length is non-significant at 25 °C. At the highest  $T$ , non-significant difference is observed in Brijis, while  $\Pi_{MAX}$  dramatically increases in  $C_{18}SE$ , reaching up to 4100 Pa against 1500 Pa at 25 °C. This is in line with the increase in film thickness with  $T$  for this surfactant. Although the average chain length only differs by 1 unit from  $C_{16}SE$  to  $C_{18}SE$ , this film thickening and the corresponding increase in  $\Pi_{MAX}$  is not observed in  $C_{16}SE$ , suggesting a strong role of stearate chains in the process.

### 3.5. Foamability and bubble size in formed foams

#### 3.5.1. Foamability in BT

The volume of entrapped air as a function of the number of shaking cycles in BT are presented in Fig. S7. The final volume of entrapped air

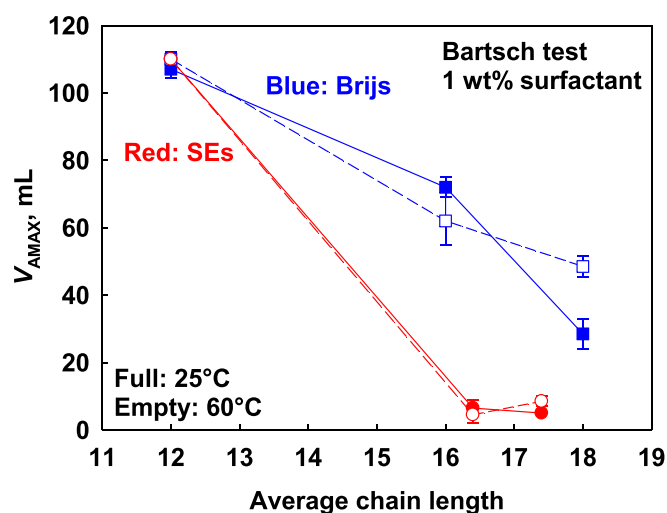


Fig. 9. Volume of entrapped air at the end of the foam generation process,  $V_{AMAX}$ , as a function of the average chain length for foams generated from 1 wt % solutions of SEs (red circles) and Brijis (blue squares) at  $T = 25$  °C (full symbols) and  $T = 60$  °C (empty symbols) in Bartsch Test after 100 shaking cycles. (For interpretation of the references to colour in this figure legend, the reader is referred to the web version of this article.)

after 100 cycles, denoted as  $V_{AMAX}$ , is presented in Fig. 9 for 1 wt% solutions, whereas the results for lower concentrations are shown in Fig. S8. It is seen that for both types of surfactants, the maximal foam volume decreases with the increase in surfactant chain length. The decrease in foamability with the increase of surfactant chain length from 12 to 14 carbon atoms is already reported in literature for alkyl benzene sulfonates homologues [82]. However, as seen from data shown in Fig. 9, the decrease also significantly depends on the surfactant head group. The decrease is more pronounced for SE surfactants, for which almost no foam is generated from both  $C_{16}SE$  and  $C_{18}SE$  sucrose esters over the whole temperature range. Compared to results obtained at lower concentrations, increasing the concentration in Brijis positively impacts the foamability, as does it in  $C_{12}SE$ , but it has no impact on long-chain sucrose esters (see Fig. S8). The inability of  $C_{16}SE$  and  $C_{18}SE$  to form voluminous foam is related to the very slow adsorption of these molecules on the solution surface and lower surface coverage, as shown in Fig. 6 above.

#### 3.5.2. Foamability in FRM

The effect of surfactant chain length on foams formed in FRM from 0.01 wt% surfactant solutions is shown in Fig. 10. For Brijis, there is no significant effect of the chain length on the amount of formed foam, but increasing the temperature significantly enhances the ability of these surfactants to retain the gas introduced into the system (see empty and full blue points in Fig. 10). On the other hand, a significant decrease in the amount of stabilized air with the increase in surfactant chain length is observed for SE surfactants at all studied temperatures at this concentration. For the 0.01 wt%  $C_{18}SE$  solution at 25 °C, the entire amount of introduced air in the solution coalesces with the atmosphere, resulting in no foam remaining at the end of the gas blowing period.

Increasing the concentration to 0.1 wt% leads to the stabilization of the entire amount of introduced gas in Brijis solutions at all temperatures. A similar effect is observed for  $C_{12}SE$  and  $C_{16}SE$  sucrose esters, but for 0.1 wt%  $C_{18}SE$  at  $T \leq 40$  °C, the coalescence between bubbles and the atmosphere remains significant, and the amount of remaining gas is lower (see Fig. S9). Further increasing the concentration to 1 wt% leads to the stabilization of gas in all studied solutions and temperatures.

#### 3.5.3. Foamability in KM

In the KM method, the solutions are sheared with a rotational speed

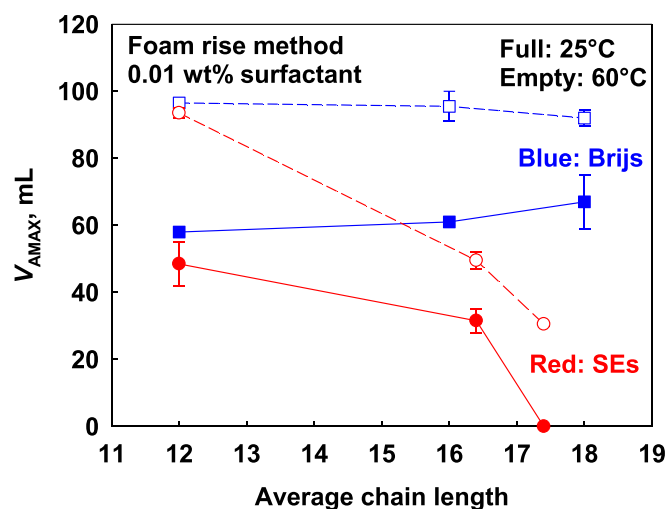


Fig. 10. Remaining air at the end of the foam generation process,  $V_{AMAX}$ , as a function of average chain length for foams generated from 0.01 wt% solutions of SEs (red circles) and Brijis (blue squares) at  $T = 25$  °C (full symbols) and  $T = 60$  °C (empty symbols) in the foam rise method after 15 s of air sparging. (For interpretation of the references to colour in this figure legend, the reader is referred to the web version of this article.)

of 2 rps, corresponding to a maximal shear rate of  $62 \text{ s}^{-1}$ , and leading to bubble formation and air entrapment. Kinetics of foam formation for 0.1 wt% and 1 wt% solutions at  $25^\circ\text{C}$  are shown in Fig. 11. In this method, the typical behavior for surfactant solutions can be divided in three steps: (i) during the induction time,  $t_{\text{IND}}$ , which is necessary to reach a certain foam height corresponding to a liquid fraction of 0.33 [49], the increase in foam volume is slow; (ii) a steeper increase in foam formation rate is observed until reaching its highest value; (iii) further shearing of the foam does not lead to further air entrapment and the volume remains constant. The induction time is shortened when increasing the concentration to 1 wt%, due to faster adsorption, and the final volume  $V_{\text{AMAX}}$  increases. Regardless of the concentration, all Brijs have very similar behavior, with similar  $V_{\text{AMAX}}$  ( $\approx 1750 \text{ mL}$ ), and similar kinetics with a slight decrease in  $t_{\text{IND}}$  for  $C_S = 1 \text{ wt\%}$ . In sucrose esters, however, increasing the chain length has a huge impact on both the kinetics and the  $V_{\text{AMAX}}$  value. As in the previous methods,  $C_{12}\text{SE}$  exhibits excellent foaming ability, with faster kinetics than Brijs and slightly higher  $V_{\text{AMAX}}$  for both concentrations. Longer chain sucrose esters present much slower kinetics, with induction times in 0.1 wt% solutions reaching  $21 \pm 2 \text{ min}$  for  $C_{16}\text{SE}$  and up to  $50 \pm 13 \text{ min}$  for  $C_{18}\text{SE}$ . For 1 wt% solutions,  $t_{\text{IND}}$  decreases to  $9.3 \pm 0.2 \text{ min}$  for  $C_{16}\text{SE}$ , and  $11.6 \pm 0.6 \text{ min}$  for  $C_{18}\text{SE}$ , but remain much higher than those of homologous Brijs.

As the plateau region is not reached even after 1 h for some of the solutions, the  $V_{\text{AMAX}}$  value is rather taken to be the calculated value  $V_{A,\infty}$ , evaluated by fitting  $V_A(t)$  data with the following expression [40]:

$$V_A = \frac{V_{A,\infty}}{1 + \exp\left(\frac{t_{50\%} - t}{t_A}\right)} \quad (7)$$

where  $V_{A,\infty}$  is the final foam volume in the plateau region,  $t_{50\%}$  is the time required to reach 50 % of  $V_{A,\infty}$ , and  $t_A$  is the rate of air entrapment for  $t = t_{50\%}$ .

### 3.5.4. Comparison between the different tests

Previous studies relate the foamability of surfactant solutions to the dynamic properties of the adsorption layer [37,40]. In particular, adsorbed layer of nonionic surfactants require a dynamic surface coverage  $\theta \geq 80\text{--}95\%$  to yield high foam volume. In ionic surfactants, electrostatic repulsion in the films additionally contribute to foam film stabilization, and substantial foam volume can be obtained for  $\theta \geq 30\%$  [37]. A recent extension of this approach was proven to predict the foamability of polymeric solutions, also considering the respective long-range steric repulsion [41]. Its applicability was verified in the case of sucrose ester  $C_{12}\text{SE}$  and  $C_{12}\text{EO}_{23}$ , at temperatures ranging from  $25^\circ\text{C}$  to  $60^\circ\text{C}$ , and in high urea content solutions [21].  $C_{12}\text{SE}$  yields high foamability for  $\theta \geq 80\%$  while  $C_{12}\text{EO}_{23}$ , in comparison, requires  $\theta \approx 95$

%. This was attributed to higher electrostatic repulsion in  $C_{12}\text{SE}$  thin liquid films as hydroxyl ions adsorb on sucrose polar heads. Greater foam stability was also reported for  $C_{12}\text{SE}$ , in relation with the higher density of the adsorbed layer [21].

To test the applicability of the proposed approach [37,40] for non-Newtonian solutions of 1 wt%  $C_{16}\text{SE}$  and  $C_{18}\text{SE}$  at high temperature and in presence of non-dissolved particles at room temperature, the relative foamability of different studied solutions were determined at different temperatures, and plotted as a function of dynamic surface coverage, see Fig. 12. The relative foamability is calculated with respect to a reference surfactant solution (50 mM sodium dodecyl sulfate, SDS), as it yields high foam volume in all methods (110 mL in BT, 95 mL in FRM, and 2070 mL in KM) [40]. The relative foamability is obtained as  $V_{\text{AMAX}}/V_{\text{AMAX}}(50 \text{ mM SDS})$  in BT and FRM, and  $V_{A,\infty}/V_{A,\infty}(50 \text{ mM SDS})$  in KM.

Results summarizing all experiments for Brij solutions are plotted in Fig. 12A as a function of dynamic surface coverage  $\theta$ . To determine the surface coverage, the characteristic adsorption time values are used:  $t_{\text{age}} = 370 \text{ ms}$  for BT [37], and  $t_{\text{age}} = 15 \text{ s}$  for KM [37,40] measured by MBPM, and  $\sim 50 \text{ s}$  for FRM measured by Wilhelmy plate method [40]. The tendency observed in Fig. 12A for Brijs is in accordance with that previously determined for nonionic surfactants (dashed line) [21,37,40]. All data at different temperature and with different foaming methods follow the same tendency.

The experimental results obtained with SEs are shown in Fig. 12B. It is seen that depending on the method used for foam generation, the experimental data for SEs followed different tendencies. The deviation of experimental data for  $C_{12}\text{SE}$  (red symbols in Fig. 12B) from the master curves for nonionic surfactants were explained in [21] by the action of long-range electrostatic repulsion due to the adsorption of  $\text{OH}^-$  ions on the hydrophilic head groups. Similar long-range electrostatic repulsion acts between bubble surfaces created in solutions of longer-chain sucrose esters ( $C_{16}\text{SE}$  and  $C_{18}\text{SE}$ ), but they are unable to ensure good foamability in BT because of very slow surfactant adsorption, which leads to surface coverage below the threshold value of 0.8, as can be seen from the data presented in Fig. 12B (full blue and green symbols). The non-Newtonian behavior of  $C_{16}\text{SE}$  and  $C_{18}\text{SE}$  solutions at high temperature additionally prevents an effective air entrapment as the solution deformation is hindered.

The threshold surface coverage of 0.8 is reached for foams formed in FRM from  $C_{16}\text{SE}$  and  $C_{18}\text{SE}$ , as can be seen from the empty green and blue symbols in Fig. 12B, but the foamability increases when the surface coverage becomes close to 1, as in the case of typical non-ionic surfactants without electrostatic repulsions. However, as shown in Fig. 8, the film thickness is even higher than that measured for  $C_{12}\text{SE}$ , indicating that hydroxyl ions are attached to the sucrose surface of  $C_{16}\text{SE}$  and  $C_{18}\text{SE}$ , but this electrostatic repulsion is not sufficient to prevent the

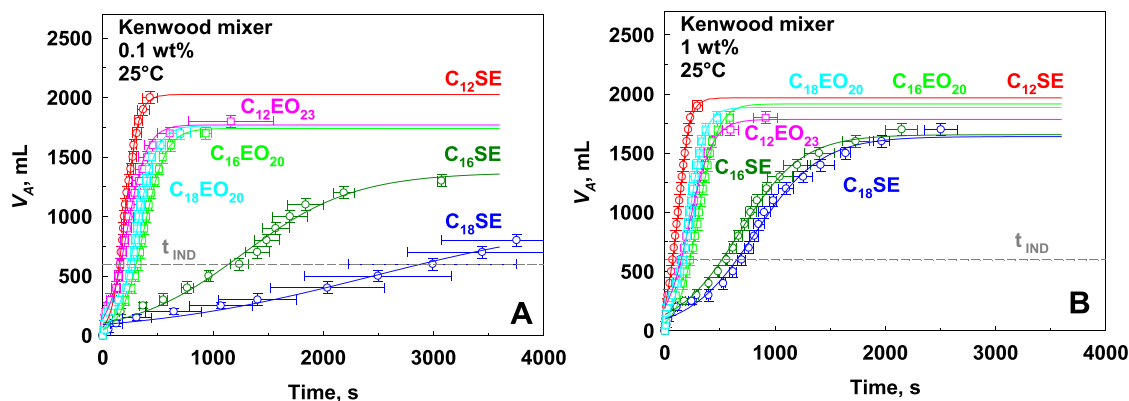
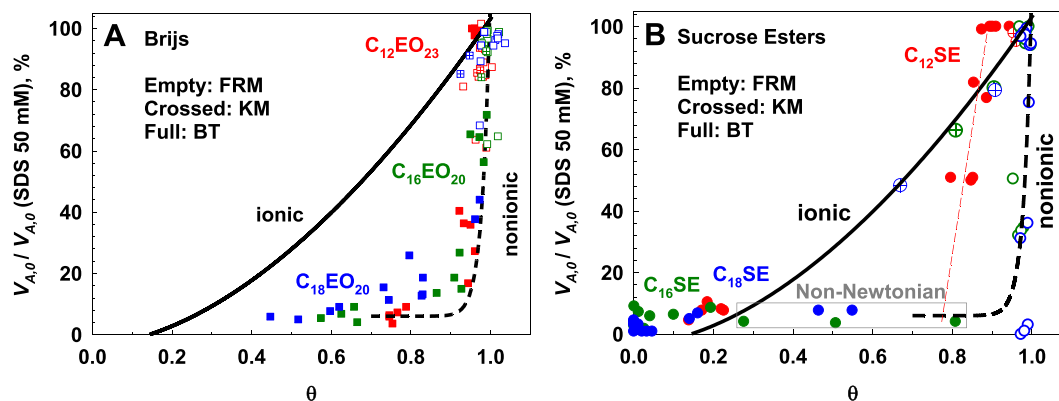


Fig. 11. Foamability at  $25^\circ\text{C}$  (A) 0.1 wt% and (B) 1 wt% solutions in the Kenwood mixer method plotted as the volume of trapped air within the foam,  $V_A$ , as a function of shearing time.



**Fig. 12.** Relative foamability compared to that of 50 mM sodium dodecyl sulfate (SDS),  $V_{A,0}/V_{A,0}(50 \text{ mM SDS})$ , as a function of dynamic surface coverage,  $\theta$ , for (A) Brij surfactants and (B) sucrose ester surfactants, formed in Bartsch test (BT), Kenwood Mixer (KM), and Foam Rise Method (FRM) at different temperatures. The master curves representing the dependence of the relative foamability for foams formed at 25 °C in different methods are taken from Ref. [83] for ionic surfactants (continuous curve), and for nonionic surfactants (dashed curve).  $\theta$  values are determined after  $t_{\text{age}} = 370 \text{ ms}$  for BT, and after  $t_{\text{age}} = 15 \text{ s}$  for KM from the MBPM, and after  $t_{\text{age}} = 50 \text{ s}$  from the Wilhelmy plate method for foams generated in FRM.

coalescence of these foams. To understand the reason for the observed discrepancy, optical observations were performed using a high-speed camera to determine the stages in foam evolution in these three sucrose ester solutions.

Massive coalescence occurs while the foam is being generated in  $C_{16}\text{SE}$  and  $C_{18}\text{SE}$  solutions using the FRM. This coalescence is related to the fact that during bubble formation, these surfactants are unable to adsorb on the bubble surface and prevent coalescence between two consecutive bubbles formed from the sparger. These bubbles coalesce with each other and form very large bubbles. This coalescence phenomenon causes the surface to expand as bubbles coalesce with each other, and the surface cannot be considered static as in the case of all other surfactants. No such coalescence is observed in  $C_{12}\text{SE}$  solutions. The most probable reason for coalescence inside the liquid between bubbles formed in longer-chain SEs ( $C_{16}\text{SE}$  and  $C_{18}\text{SE}$ ) is their very slow adsorption on the bubble surfaces in the initial stage of bubble generation (see Fig. 4 above). Note that for Brij solutions, the lag time for surfactant adsorption at 0.01 wt% is around 100 times shorter than the lag time for  $C_{16}\text{SE}$  and  $C_{18}\text{SE}$ , showing that the surface coverage of the bubbles traveling in long-chain Brij surfactants is sufficient to prevent bubble–bubble coalescence inside the liquid, whereas it is not for SEs.

On the other hand, the experimental data for foams generated in KM after a prolonged period of mixing of long-chain SEs lay on the master curve of ionic surfactants (see crossed symbols in Fig. 12B). This particular effect can be explained by the very long mixing time required to produce foams from those solutions (see Fig. 11A). During this mixing, significant accumulation of diester molecules on the bubble surfaces occurs, and as a consequence, the electrostatic repulsion becomes more pronounced and the required surface coverage decreases. It should be mentioned that the surface coverage is calculated based on surface tension isotherms measured after 10 min, whereas, with this prolonged mixing, the composition of the adsorption layer is changed and the characteristics of adsorption layers are different, as shown in Fig. S3D in the supporting information. The fact that SEs align with the master curve for nonionic surfactants when foams are prepared in FRM, but follow the master curve for ionic surfactants when foams are prepared using the KM method, can be explained by the differences in the composition of the adsorption layers formed on bubble surfaces in each foaming method. In FRM, the hydrodynamic conditions are milder and particles containing diester molecules cannot adsorb on the bubble surface, whereas in KM the mixing is sufficient to allow the adsorption of diester molecules after prolonged mixing. However, for determining the surface coverage in both methods, the considered characteristics referred to layers in which monoesters prevail on the surface. Therefore, the fact that data for SE foams formed in KM followed the trend for ionic

surfactant could be related to the inaccurate determination of the bubble surface coverage due to the accumulation of diester molecules, or/and to the adsorption of hydroxyl ions giving rise to higher electrostatic repulsion between the bubble surfaces in the presence of adsorbed diester molecules.

As a summary of the foaming data, it can be concluded that the approach developed in [37] and applied in [21,40] can be used for foams formed from Brij surfactants in different tests and temperatures. For all of them, the short-range steric repulsion is required for foam stabilization, and the threshold surface coverage is approximately 95 %. For sucrose ester surfactants that have very slow adsorption ( $C_{16}\text{SE}$  and  $C_{18}\text{SE}$ ), coalescence starts during bubble generation in all tests. For FRM and BT, where the mixing time is short and no accumulation of diesters is possible on the bubble surfaces during their formation, the threshold surface coverage for foam stabilization becomes very close to that determined for non-ionic surfactants with short-range steric repulsion. For foams formed in KM, where prolonged mixing is applied, diester accumulation is possible, and the threshold surface coverage becomes even lower compared to that determined for  $C_{12}\text{SE}$ , in agreement with thicker films observed in the capillary cell, see Fig. 7.

### 3.5.5. Bubble size

The three investigated methods differ significantly in the way bubbles are formed: while the bubble size is mostly governed by the membrane type and the flow rate in FRM, bubbles are formed by shearing in BT and in KM. Macroscopic pictures of foams formed at 25 °C are shown in Fig. 13A (FRM) and Fig. S10 (KM and BT), and  $R_V(50)$  values in the three methods for 1 wt% solutions are compared in Fig. 13B. One can notice the foams generated in KM have smaller bubbles, with little variations from one surfactant to another.

In FRM foams, the evolution tendency with the alkyl chain length is identical among SEs and Brij surfactants:  $R_V(50)$  increases with the alkyl chain length. Although  $R_V(50)$  values are similar for  $C_{12}$  surfactants, they differ significantly among  $C_{16}$  and  $C_{18}$  surfactants of both groups, with larger  $R_V(50)$  in sucrose esters. Differences are so striking that they can be macroscopically observed, see Fig. 13A. As the surface is slowly stabilized, bubbles can easily coalesce with each other before reaching the surface, or within the foam column. From Fig. S11, it is seen that the initially formed bubbles on the FRM membrane are about the size of 100  $\mu\text{m}$  or below for all three sucrose esters, which hardly corresponds to the size of the finally obtained bubbles in the foam column, reaching over 1 cm in the case of 0.1 wt%  $C_{18}\text{SE}$  (see Fig. 13A). The experiments in Fig. S11 were conducted to understand whether large bubbles were formed directly on the membrane in the case of  $C_{16}\text{SE}$  and  $C_{18}\text{SE}$ , or whether if small bubbles coalesced to yield the very large final size. This

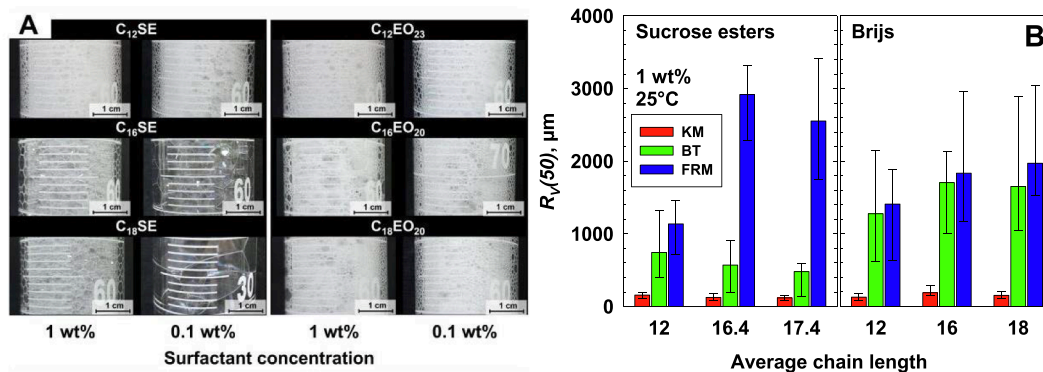


Fig. 13. (A) Macroscopic pictures of foams generated at 25 °C using the FRM, and (B) volume median bubble radius,  $R_V(50)$ , for foams prepared at 25 °C by KM, BT, and FRM, using 1 wt% solutions of sucrose esters or Brijis of varying alkyl chain length. Lower and upper error bars correspond to  $R_V(16)$  and  $R_V(84)$ , respectively.

last explanation was confirmed, and high-speed observation of the foam column during FRM air sparging showed coalescence of bubbles between them within the liquid which afterwards facilitate their coalescence with atmosphere.

### 3.6. Foam stability after stopping the foam generation

The rate of foam destruction after stopping the agitation depends on three main processes: (1) water drainage, (2) Ostwald ripening, and (3) bubble–bubble and bubble–atmosphere coalescence. The Ostwald ripening and bubble–bubble coalescence result in an increase of mean bubble size within the foam, whereas the water drainage increases the local air volume fraction and, in such way, increases the film area

between two bubbles or between bubble and surrounding atmosphere at a given bubble size [84] and decreases the film thickness. Both the increase of bubble size and the increase of film area lead to higher probability for coalescence events. The processes of water drainage and Ostwald ripening depend on both bulk and surface properties: the increase of solution viscosity decreases the water drainage and the gas transfer from smaller to bigger bubbles, and the formation of condensate adsorption layers on the bubble surfaces also diminishes the rate of these two processes [85–89]. In order to decouple the effect of the surfactant type and that of the bubble size on the destabilization kinetics, experiments were conducted with a fixed type of surfactant (C<sub>12</sub>SE), and the size of formed bubbles was varied (section 3.6.1). The stability of formed foams was then evaluated. In a second series of experiments the bubble

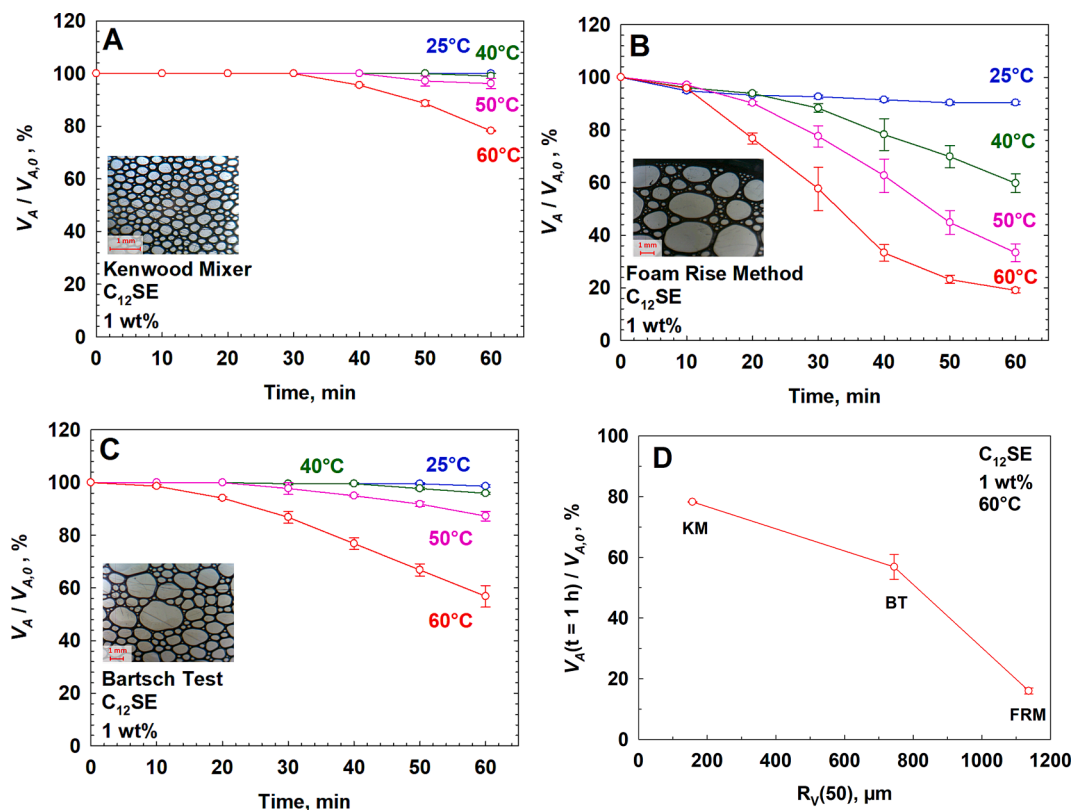


Fig. 14. Relative foam stability over 1 h, defined as the ratio between the instantaneous volume of trapped air and the initial volume of trapped air immediately after foam formation,  $V_A/V_{A,0}$ , for foams obtained using 1 wt% L1695 solution in Kenwood Mixer (A), Foam rise method (B), and Bartsch Test (C), at different temperatures, and (D) relative foamability after 1 h at 60 °C as a function of bubble size,  $R_V(50)$ . Inserted pictures correspond to foams observed at 25 °C using the Garrett method.

size was fixed, and the type of surfactant used for their stabilization was varied (section 3.6.2).

### 3.6.1. Impact of the bubble size on $C_{12}SE$ foam stability

In our previous study,  $C_{12}SE$  foams were investigated in BT and FRM. In this study, further interest was set on 1 wt%  $C_{12}SE$  foams as no destabilization was observed within 10 min when prepared by FRM or BT. Additional destabilization monitoring was then continued for 1 h, and compared to the foam prepared by KM under the same conditions. The corresponding kinetics of destabilization are shown in Fig. 14.

Foams formed in BT and in KM from 1 wt%  $C_{12}SE$  remain stable over 1 h at 25 °C and the entire foam volume is maintained. In FRM, a slight volume decrease is seen, but the kinetics is very slow and  $\approx 90\%$  of the initial volume is maintained after 1 h.

It is known that increasing the temperature has a significant effect on the foam properties, and that stability decreases with temperature for all types of surfactants (anionic, cationic, nonionic, and amphoteric) [21,34,90,91]. That is why the effect of temperature on foams prepared using  $C_{12}SE$  solutions was investigated in three different methods. It is observed that foam stability decreases with increasing temperature for foams formed in all different methods. This effect is most pronounced for foams formed in FRM, and least for those formed in KM. This difference is related to two effects: (1) Bigger bubbles and (2) Higher polydispersity of foams formed in FRM compared to KM. As a result, both coalescence and Ostwald ripening are more prominent in foams formed in FRM at elevated temperatures. Larger bubbles are less stable against coalescence, while higher polydispersity accelerates the Ostwald ripening process, which becomes very pronounced at higher temperature as the viscosity decreases. The better stability of foams formed in the KM compared to those formed in FRM is at least partially due to the milder conditions during foam generation in FRM, preventing diester molecules from adsorbing onto the bubble surfaces. In contrast, the more thorough mixing during foam generation in KM promotes the adsorption of diester molecules on the bubble surface, slowing down Ostwald ripening, and enhancing foam stability even at higher temperatures.

It is known from the literature that foams with larger bubbles destabilize faster and are more prompt to coalesce than foams with smaller ones [92–94]. Drainage is slower in foams with smaller bubbles [95], and larger bubbles are most likely to cause avalanche phenomena when bursting: the bursting of one large bubble triggers a larger variation in liquid fraction, that in turn destabilizes plateau regions of bubbles underneath [95–97]. Also, the probability of film rupture is proportional to its area, since the failure of a single point on the film is sufficient to cause rupture [98]. Consequently, foams with larger bubbles are more subject to faster destabilization. However, as it was shown in [99], the destabilization of foams containing small bubbles occurs during reorganization events (so called T1 events) induced by bubble

coarsening, which is particularly rapid in the case of small bubbles. Therefore, sucrose ester surfactants are also able to impact T1 events in the foams, efficiently stabilizing foams with small bubbles as well.

### 3.6.2. Stability of foams with similar initial bubble size

The experimental results shown in Fig. 15 are obtained with foams generated in KM under equivalent conditions for all surfactants. These foams have an initial bubble size between 100 and 150  $\mu\text{m}$ . The rate of foam destruction is very fast in Brij stabilized foams, especially at elevated temperatures, whereas the foams formed from SEs surfactants remain very stable even after 1 h of storage at 60 °C. In order to determine the effect of surfactant chain length on the foam stability, the foam half time was determined for foams obtained from 1 wt% Brij solutions and stored at 40 °C, see Fig. 15B. The increase of chain length for Brij surfactants increases the time required for their destabilization. The similar effect is expected for SEs foams, but the monitoring time was not sufficient to observe the destruction of the formed foams even at the highest temperature.

The viscous effect contributes to slowing down drainage and film thinning. This phenomenon is illustrated by the comparative evolution of  $C_{16}EO_{20}$  and  $C_{16}SE$  foams formed in KM with 0.1 wt% and 1 wt% solutions and stored at 50 °C, see Figure S12. While the low-viscous solutions are almost totally drained within 10 min, the shear-thinning solutions in 1 wt%  $C_{16}SE$  is not totally drained after 60 min, reaching only  $\approx 70\%$  of the total solution volume. Note that the drainage is very fast in 0.1 wt%  $C_{16}SE$  which exhibits Newtonian behavior. This means that  $C_{16}SE$  films remain thicker for longer. Besides impacting the foam film thickness, bulk viscosity also slows down the rate of Ostwald ripening [85–87]. It is seen from the evolution of the foam column that bubble evolution is slow: the column remains opaque, indicating little bubble size evolution, and the overall foam volume remains constant over 60 min. Interestingly, 1 wt%  $C_{16}SE$  foams prepared in KM show a slightly better stability than those from 1 wt%  $C_{18}SE$ . This is explained by the higher low-shear viscosity of  $C_{16}SE$  solutions at 40 °C, 50 °C, and 60 °C compared to those of 1 wt%  $C_{18}SE$  solutions in similar conditions. This phenomenon is well-known for surfactant solutions forming worm-like micelles and other high-viscosity solutions [24,88].

### 3.6.3. Stability of foams formed in FRM and in BT having different bubble sizes

For all samples, the foam decay was monitored over 10 min for BT and FRM, see Figures S13–S18. Values of the relative amount of air remaining in the foams after the decay for 1 wt% solutions are presented in Fig. 16.

The foams formed from  $C_{16}SE$  and  $C_{18}SE$  remain stable over the  $T$  range when they are formed in BT, and significant decrease in foam stability is observed for foams formed from these solutions in FRM, see

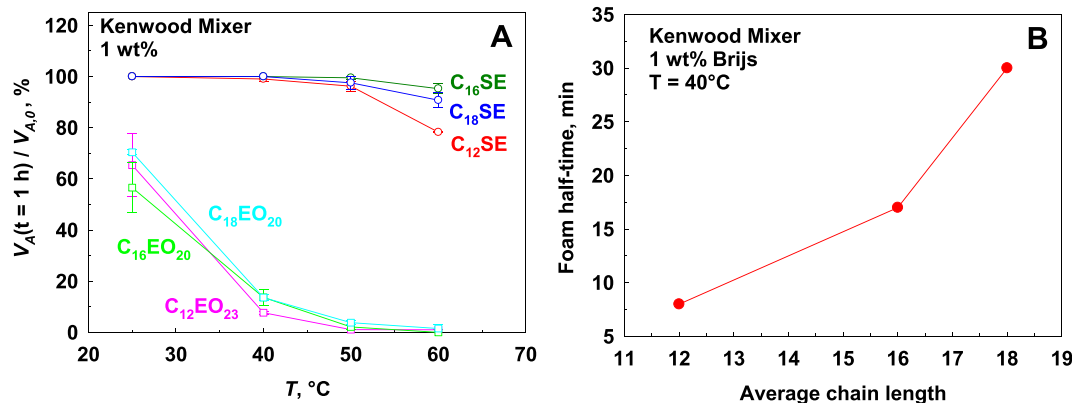
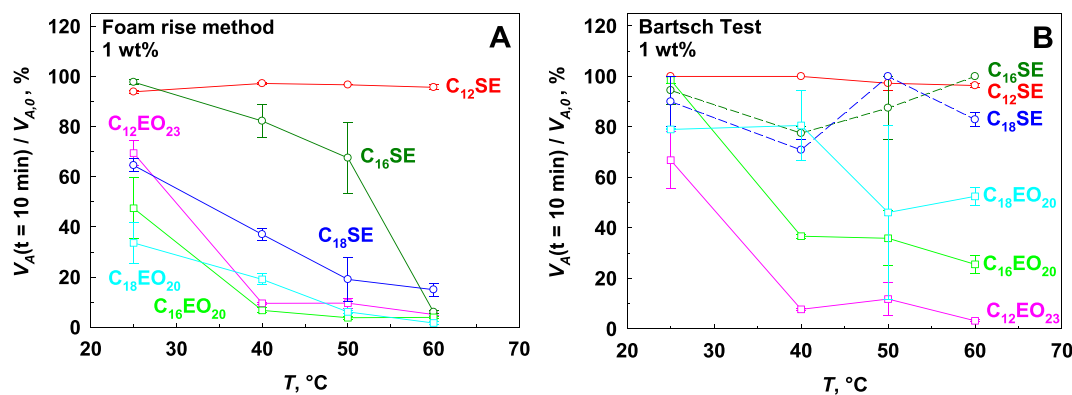


Fig. 15. (A) Relative remaining volume of air entrapped in the foam after 1 h of storage as a function of temperature,  $T$ , for foams generated with 1 wt% solutions in Kenwood Mixer, KM. (B) Foam half-time as a function of average chain length for foams formed from 1 wt% Brij solutions in KM.



**Fig. 16.** Relative remaining volume of air entrapped in the foam at the end of decay monitoring as a function of temperature,  $T$ , for foams generated with 1 wt% solutions in (A) FRM, and (B) BT. The final time is taken to be 10 min in both methods.

**Fig. 16.** This is related to different bubble size on one side, and different adsorption layers on the other side. The bubbles in foams formed in FRM are much bigger than those in foams formed in BT, see Fig. 13B above.

This also partially accounts for the difference in Brij's foams stability at 25 °C in FRM: 1 wt%  $C_{16}EO_{20}$  and  $C_{18}EO_{20}$  foams are less stable than the  $C_{12}EO_{23}$  ones, in accordance with the tendency in  $R_V(50)$  differences for this surfactant series, see Fig. 13B. The differences in stability among the Brij series fade with increasing  $T$  as films get thinner and rupture much more easily. For both surfactant series, the foams generated with 1 wt% solutions in FRM are more stable with  $C_{12}$  surfactants, and the decreasing stability over increasing the chain length is accounted for by differences in bubble size. When bubble sizes are similar, as it is the case in KM foams, chain length has positive impact on foam stability as can be seen from Fig. 15B above.

#### 4. Conclusions

Systematic series of experiments aimed at determining the effect of surfactant chain length on the solution, surface, film and foam properties of alkyl sucrose esters, SEs, and alkyl polyoxyethylene ethers, Brij's, were performed at different temperatures between 25 °C and 60 °C, and concentrations between 0.01 wt% and 1 wt%. The viscosity of Brij's solutions does not depend on the surfactant chain length and decreases with the temperature increase, whereas the temperature increase triggers the formation of worm-like micelles in 1 wt% solutions of long chain sucrose esters, namely  $C_{16}SE$  and  $C_{18}SE$ . The increase of chain length increases the temperature at which the worm-like micelles are formed.

Critical micellar concentration (CMC) for Brij's decreases with the increase of alkyl chain length and temperature. Similar decrease is determined for  $C_{12}SE$  and  $C_{16}SE$ , whereas further increase of surfactant chain length for  $C_{18}SE$  has almost no effect on CMC at 25 °C due to the presence of particles that incorporated insoluble molecules. Higher temperatures lead to a significant decrease in the CMC for  $C_{18}SE$ , and almost linear dependence between  $\ln(\text{CMC})$  and the number of carbon atoms in surfactant tails, due to the melting of solid particles and incorporation of diesters in surfactant micelles.

The surfactant adsorption increases with temperature for SEs and decreases for Brij's. The increase of surfactant chain length at a given temperature increases the adsorption for SEs and slightly decreases the adsorption for Brij's. In the case of SEs, this is explained by the incorporation of a higher amount of diesters on the air–water interface at higher temperatures and with longer tails. The thickness of foam films increases with temperature and chain length for SEs and the opposite trends are determined for Brij's. The decreased thickness is related to lower adsorption of hydroxyl ions at higher temperature for Brij's surfactants, whereas the adsorption of diesters provoke a further increase in hydroxyl ions presence, and larger film thickness for SEs. For the first

time, the cyclic dimple formation was observed in foam films formed with non-volatile surfactants, in relation with different compositions of adsorption layers on film surfaces and on meniscus surfaces due to a different re-distribution of diester molecules.

The foaming properties of SEs solutions are highly sensitive to the method used for foam generation: the foams formed in foam rise method from 0.1 wt% solutions of long chain SEs lead to the formation of very big bubbles due to the tremendous coalescence between the bubbles as they travel through the liquid. This effect is not observed for the shorter chain sucrose ester nor for all the studied Brij's, and is explained by the very long lag time determined from the dynamic surface tension measurements. On the other hand, voluminous foams with small bubbles are formed in Kenwood mixer when prolonged mixing is applied. When foams with similar bubble sizes are investigated, much better stability is achieved with SEs compared to Brij's, especially at higher temperatures, and increasing the chain length further improves foam stability.

#### CRediT authorship contribution statement

**L. Delforce:** Writing – original draft, Visualization, Investigation, Formal analysis, Data curation. **S. Tcholakova:** Writing – review & editing, Supervision, Methodology, Funding acquisition, Formal analysis, Conceptualization.

#### Funding

This study is financed by the European Union-Next Generation EU, through the National Recovery and Resilience Plan of the Republic of Bulgaria, project N<sup>o</sup> BG-RRP-2.004-0008-C01.

#### Declaration of competing interest

The authors declare that they have no known competing financial interests or personal relationships that could have appeared to influence the work reported in this paper.

#### Acknowledgements

The authors thank Nevena Pagureva, Vasil Georgiev, and Dora Dimitrova (Sofia University) for their assistance in surface tension and foaming techniques. We are also grateful to Vladimir Petkov (Sofia University) for chromatography analyses.

Our gratitude goes to Mitsubishi Chemical Corporation for the generous donation of L1695 and S1570 Ryoto<sup>TM</sup> sucrose esters, allowing us to perform this study.

## Appendix A. Supplementary data

Supplementary data to this article can be found online at <https://doi.org/10.1016/j.molliq.2024.126491>.

## Data availability

Data will be made available on request.

## References

1. R. Farajzadeh, A. Andrianov, R. Krastev, G.J. Hirasaki, W.R. Rossen, Foam-oil interaction in porous media: Implications for foam assisted enhanced oil recovery, *Adv. Colloid Interface Sci.* 183–184 (2012) 1–13, <https://doi.org/10.1016/j.cis.2012.07.002>.
2. Q. Sun, Zh. Li, S. Li, L. Jiang, J. Wang, P. Wang, Utilization of surfactant-stabilized foam for enhanced oil recovery by adding nanoparticles, *Energy Fuels* 28 (2014) 2384–2394, <https://doi.org/10.1021/ef402453b>.
3. N. Pal, A. Verma, K. Ojha, A. Mandal, Nanoparticle-modified gemini surfactant foams as efficient displacing fluids for enhanced oil recovery, *J. Mol. Liq.* 310 (2020) 113193, <https://doi.org/10.1016/j.molliq.2020.113193>.
4. K.R. Chaturvedi, R. Narukulla, J. Trivedi, T. Sharma, Effect of single-step silica nanoparticle on rheological characterization of surfactant based CO<sub>2</sub> foam for effective carbon utilization in subsurface applications, *J. Mol. Liq.* 341 (2020) 116905, <https://doi.org/10.1016/j.molliq.2021.116905>.
5. S. Babamahmoudi, S. Riahi, Application of nano particle for enhancement of foam stability in the presence of crude oil: Experimental investigation, *J. Mol. Liq.* 264 (2018) 499–509, <https://doi.org/10.1016/j.molliq.2018.04.093>.
6. J.M. Rodríguez Patino, M. Dolores Naranjo Delgado, J. Linares Fernández, Stability and mechanical strength of aqueous foams containing food proteins, *Colloids Surf. A Physicochem. Eng. Asp.* 99 (1995) 65–78, [https://doi.org/10.1016/0927-7757\(95\)03129-2](https://doi.org/10.1016/0927-7757(95)03129-2).
7. H.D. Goff, C. Vega, Structure-engineering of ice-cream and foam-based foods. In *Understanding and Controlling the Microstructure of Complex Foods*, Woodhead Publishing Series in Food Science, Technology and Nutrition (2007) 557–574, [https://doi.org/10.1533/9781845693671\\_4.557](https://doi.org/10.1533/9781845693671_4.557).
8. R. Zheng, X. Hu, Ch. Su, J. Jiang, Zh. Cui, B.P. Binks, Edible oil-water foams stabilized by vesicle network of sucrose ester, *J. Mol. Liq.* 371 (2023) 121066, <https://doi.org/10.1016/j.molliq.2022.121066>.
9. J. Lehmonen, T. Rantanen, K. Kinnunen-Raudaskoski, Upscaling of foam forming technology for pilot scale. *Tappi J.* 18(8) (2019) 461–471, <https://doi.org/10.32964/TJ18.8.461>.
10. R. Hasanzadeh, T. Azdast, P.C. Lee, C.B. Park, A review of the state-of-the-art on thermal insulation performance of polymeric foams, *Thermal Science and Engineering Progress* 41 (2023) 101808, <https://doi.org/10.1016/j.tsep.2023.101808>.
11. R. Hasanzadeh, T. Azdast, A. Doniavi, P.C. Lee, Multi-objective optimization of heat transfer mechanisms of microcellular polymeric foams from thermal-insulation point of view, *Thermal Science and Engineering Progress* 9 (2019) 21–29, <https://doi.org/10.1016/j.tsep.2018.11.002>.
12. A.L. Brooks, Z. Shen, H. Zhou, Development of a high-temperature inorganic synthetic foam with recycled fly-ash cenospheres for thermal insulation brick manufacturing, *J. Clean Prod.* 246 (2020) 118748, <https://doi.org/10.1016/j.jclepro.2019.118748>.
13. H. Alghamdi, N. Neithalath, Synthesis and characterization of 3D-printable geopolymeric foams for thermally efficient building envelope materials, *Cem. Concr. Compos.* 104 (2019) 103377, <https://doi.org/10.1016/j.cemconcomp.2019.103377>.
14. M. Hristova, I. Lesov, L. Mihaylov, N. Denkov, S. Tcholakova, Role of particle size on the cohesive strength of non-sintered (green) ceramics, *Colloids Surf. A Physicochem. Eng. Asp.* 658 (2023) 130653, <https://doi.org/10.1016/j.colsurfa.2022.130653>.
15. M. Hristova, I. Lesov, S. Tcholakova, V. Goletto, N. Denkov, From Pickering foams to porous carbonate materials: Crack-free structuring in drying ceramics, *Colloids Surf. A Physicochem. Eng. Asp.* 552 (2018) 142–152, <https://doi.org/10.1016/j.colsurfa.2018.05.025>.
16. N.S. Neta, J.A. Teixeira, L.R. Rodrigues, Sugar Ester Surfactants: Enzymatic Synthesis and Applications in Food Industry, *Crit. Rev. Food Sci. Nutr.* 55 (2015) 595–610, <https://doi.org/10.1080/10408398.2012.667461>.
17. B.A.P. Nelen, L. Bax, J.M. Cooper, Sucrose Esters, in: *Emulsifiers in Food Technology*, John Wiley & Sons, Ltd, 2014: pp. 147–180. <https://doi.org/10.1002/9781118921265.ch7>.
18. G. Garofalakis, B.S. Murray, Dilatational rheology and foaming properties of sucrose monoesters in the presence of  $\beta$ -lactoglobulin, *Colloids Surf. B Biointerfaces* 21 (2001) 3–17, [https://doi.org/10.1016/S0927-7765\(01\)00179-5](https://doi.org/10.1016/S0927-7765(01)00179-5).
19. Y. Liu, B.P. Binks, A novel strategy to fabricate stable oil foams with sucrose ester surfactant, *J. Colloid Interface Sci.* 594 (2021) 204–216, <https://doi.org/10.1016/j.jcis.2021.03.021>.
20. F.A. Husband, D.B. Sarney, M.J. Barnard, P.J. Wilde, Comparison of foaming and interfacial properties of pure sucrose monolaurates, dilaurate and commercial preparations, *Food Hydrocoll.* 12 (1998) 237–244, [https://doi.org/10.1016/S0268-005X\(98\)00036-8](https://doi.org/10.1016/S0268-005X(98)00036-8).
21. L. Delforce, S. Tcholakova, Role of temperature and urea for surface and foam properties of nonionic surfactants with dodecyl alkyl chain, *Colloids Surf. A Physicochem. Eng. Asp.* 691 (2024) 133844, <https://doi.org/10.1016/j.colsurfa.2024.133844>.
22. S. Soltani, S. Ognier, J.-M. Engasser, M. Ghoul, Comparative study of some surface active properties of fructose esters and commercial sucrose esters, *Colloids Surf. A Physicochem. Eng. Asp.* 227 (2003) 35–44, [https://doi.org/10.1016/S0927-7757\(03\)00360-1](https://doi.org/10.1016/S0927-7757(03)00360-1).
23. S.E.H.J. Van Kempen, H.A. Schols, E. Van Der Linden, L.M.C. Sagis, Effect of Variations in the Fatty Acid Chain of Oligofructose Fatty Acid Esters on Their Foaming Functionality, *Food Biophys.* 9 (2013) 114–124, <https://doi.org/10.1007/s11483-013-9324-1>.
24. F. Mustan, N. Politova-Brinkova, Z. Vinarov, D. Rossetti, P. Rayment, S. Tcholakova, Interplay between bulk aggregates, surface properties and foam stability of nonionic surfactants, *Adv. Colloid Interface Sci.* 302 (2022) 102618, <https://doi.org/10.1016/j.cis.2022.102618>.
25. E. Dressaire, R. Bee, D.C. Bell, A. Lips, H.A. Stone, Interfacial Polygonal Nanopatterning of Stable Microbubbles, *Science* 320 (2008) 1198–1201, <https://doi.org/10.1126/science.1154601>.
26. K.W. Dillan, Effects of the ethylene oxide distribution on nonionic surfactant properties, *J. Am. Oil Chem. Soc.* 62 (1985) 1144–1151, <https://doi.org/10.1007/BF02542311>.
27. T. Tamura, Y. Kaneko, M. Ohyama, Dynamic Surface Tension and Foaming Properties of Aqueous Polyoxyethylene n-Dodecyl Ether Solutions, *J. Colloid Interface Sci.* 173 (1995) 493–499, <https://doi.org/10.1006/jcis.1995.1351>.
28. S. Yada, T. Suzuki, S. Hashimoto, T. Yoshimura, Adsorption and Aggregation Properties of Homogeneous Polyoxypropylene-Polyoxyethylene Alkyl Ether Type Nonionic Surfactants, *Langmuir* 33 (2017) 3794–3801, <https://doi.org/10.1021/acs.langmuir.7b00104>.
29. D.J. Mitchell, G.J.T. Tiddy, L. Waring, T. Bostock, M.P. McDonald, Phase behaviour of polyoxyethylene surfactants with water. Mesophase structures and partial miscibility (cloud points), *J. Chem. Soc., Faraday Trans. 1*, 79 (1983) 975–1000. <https://doi.org/10.1039/F19837900975>.
30. L.-J. Chen, S.-Y. Lin, C.-C. Huang, E.-M. Chen, Temperature dependence of critical micelle concentration of polyoxyethylenated non-ionic surfactants, *Colloids Surf. A Physicochem. Eng. Asp.* 135 (1998) 175–181, [https://doi.org/10.1016/S0927-7757\(97\)00238-0](https://doi.org/10.1016/S0927-7757(97)00238-0).
31. Z.-L. Chen, Y.-L. Yan, X.-B. Huang, Stabilization of foams solely with polyoxyethylene-type nonionic surfactant, *Colloids Surf. A Physicochem. Eng. Asp.* 331 (2008) 239–244, <https://doi.org/10.1016/j.colsurfa.2008.08.011>.
32. A. Berthod, S. Tomer, J.G. Dorsey, Polyoxyethylene alkyl ether nonionic surfactants: physicochemical properties and use for cholesterol determination in food, *Talanta* 55 (2001) 69–83, [https://doi.org/10.1016/S0039-9140\(01\)00395-2](https://doi.org/10.1016/S0039-9140(01)00395-2).
33. A.N. Wrigley, F.D. Smith, A.J. Stirton, Synthetic detergents from animal fats. VIII. The ethoxylation of fatty acids and alcohols, *J. Am. Oil Chem. Soc.* 34 (1957) 39–43, <https://doi.org/10.1007/BF02637936>.
34. H. Wang, W. Guo, C. Zheng, D. Wang, H. Zhan, Effect of Temperature on Foaming Ability and Foam Stability of Typical Surfactants Used for Foaming Agent, *J. Surfactants Deterg.* 20 (2017) 615–622, <https://doi.org/10.1007/s11743-017-1953-9>.
35. A. Bonfillon-Colin, D. Langevin, Why Do Ethoxylated Nonionic Surfactants Not Foam at High Temperature? *Langmuir* 13 (1997) 599–601, <https://doi.org/10.1021/la950439i>.
36. M.J. Rosen, J.T. Kunjappu, *Surfactants and interfacial phenomena*, 4th ed, Wiley, Hoboken, N.J., 2012.
37. M.J. Schick, E.A. Beyer, Foaming properties of nonionic detergents, *J. Am. Oil Chem. Soc.* 40 (1963) 66–68, <https://doi.org/10.1007/BF02654745>.
38. B. Petkova, M. Chenkova, K. Golemanov, N. Denkov, S. Tcholakova, D. Thorley, S. Stoyanov, Foamability of aqueous solutions: Role of surfactant type and concentration, *Adv. Colloid Interface Sci.* 276 (2020) 102084, <https://doi.org/10.1016/j.cis.2019.102084>.
39. J. Boos, W. Drenckhan, C. Stubenrauch, Protocol for Studying Aqueous Foams Stabilized by Surfactant Mixtures, *J. Surfactants Deterg.* 16 (2013) 1–12, <https://doi.org/10.1007/s11743-012-1416-2>.
40. L. Delforce, V. Nardello-Rataj, R. Lebeuf, J.-M. Aubry, J.F. Ontiveros, Self-aggregation, dilatational surface rheology and foaming properties of 1-O-dodecyl diglycerol ether compared to n-dodecyl- $\beta$ -D-maltoside and pentaerythritol monododecyl ether, *J. Mol. Liq.* 388 (2023) 122795, <https://doi.org/10.1016/j.molliq.2023.122795>.
41. B. Petkova, S. Tcholakova, N. Denkov, Foamability of surfactant solutions: Interplay between adsorption and hydrodynamic conditions, *Colloids Surf. A Physicochem. Eng. Asp.* 626 (2021) 127009, <https://doi.org/10.1016/j.colsurfa.2021.127009>.
42. V. Georgiev, Z. Mitrova, N. Genchev, A. Gers-Barlag, G. Jaunky, N. Denkov, S. Tcholakova, Surface and foam properties of polyvinyl alcohol solutions, *Colloids Surf. A Physicochem. Eng. Asp.* 681 (2024) 132828, <https://doi.org/10.1016/j.colsurfa.2023.132828>.
43. G.C. Sawicki, Silicone polymers as foam control agents, *J. Am. Oil Chem Soc.* 65 (1988) 1013–1016, <https://doi.org/10.1007/BF02544531>.
44. Th. Croguennec, A. Renault, S. Beaufils, J.-J. Dubois, S. Pezennec, Interfacial properties of heat-treated ovalbumin, *J. Colloid Interface Sci.* 315 (2007) 627–636, <https://doi.org/10.1016/j.jcis.2007.07.041>.
45. V. Raikos, L. Campbell, S.R. Euston, Effects of sucrose and sodium chloride on foaming properties of egg white proteins, *Food Res. Int.* 40 (2007) 347–355, <https://doi.org/10.1016/j.foodres.2006.10.008>.
46. Mitsubishi Chemical Corporation, Physical properties of Sugar Esters, (n.d.). <https://www.mfc.co.jp/english/physical.htm> (accessed January 12, 2024).

- [47] A.-S. Muller, J. Gagnaire, Y. Queneau, M. Karaoglanian, J.-P. Maitre, A. Bouchu, Winsor behaviour of sucrose fatty acid esters: choice of the cosurfactant and effect of the surfactant composition, *Colloids Surf. A Physicochem. Eng. Asp.* 203 (2002) 55–66, [https://doi.org/10.1016/S0927-7757\(01\)01067-6](https://doi.org/10.1016/S0927-7757(01)01067-6).
- [48] D. Cholokova, S. Tcholakova, Sucrose ester surfactants: Current understanding and emerging perspectives, *Curr. Opin. Colloid Interface Sci.* 73 (2024) 101832, <https://doi.org/10.1016/j.cocis.2024.101832>.
- [49] A. Sheludko, Thin liquid films, *Adv. Colloid Interface Sci.* 1 (1967) 391–464, [https://doi.org/10.1016/0001-8686\(67\)85001-2](https://doi.org/10.1016/0001-8686(67)85001-2).
- [50] N. Politova, S. Tcholakova, Z. Valkova, K. Golemanov, N.D. Denkov, Self-regulation of foam volume and bubble size during foaming via shear mixing, *Colloids Surf. A Physicochem. Eng. Asp.* 539 (2018) 18–28, <https://doi.org/10.1016/j.colsurfa.2017.12.006>.
- [51] P.R. Garrett, J.D. Hines, S.C. Joyce, P.T. Whittall, Report prepared for Unilever R&D, Port Sunlight, UK, 1993.
- [52] Sucrose Fatty Acid Ester | TCI AMERICA, (n.d.). <https://www.tcichemicals.com/US/en/p/S0112> (accessed January 24, 2024).
- [53] C. Calahorra, J. Muñoz, M. Berjano, A. Guerrero, C. Gallegos, Flow behavior of sucrose stearate/water systems, *J. Am. Oil Chem. Soc.* 69 (1992) 660–666, <https://doi.org/10.1007/BF02635806>.
- [54] S. Takahashi, I. Kaneda, A Transient Network Structure in Sucrose Stearate/Water Systems, *J. Soc. Rheol., Jpn* 42 (2014) 103–109, <https://doi.org/10.1678/rheology.42.103>.
- [55] N. Pagureva, D. Cholokova, Z. Mitrinova, M. Hristova, N. Burdziev, S. Tcholakova, Temperature response of sucrose palmitate solutions: Role of ratio between monoesters and diesters, *J. Colloid Interface Sci.* 674 (2024) 209–224, <https://doi.org/10.1016/j.jcis.2024.06.061>.
- [56] P.A. Kralchevsky, K.D. Danov, N.D. Denkov, Chemical Physics of Colloid Systems and Interfaces, in: K.S. Birdi (Ed.), *Handbook of Surface and Colloid Chemistry*, 3rd ed., CRC Press, 2008.
- [57] K.J. Mysels, Surface tension of solutions of pure sodium dodecylsulfate, *Langmuir* 2 (1986) 423–428, <https://doi.org/10.1021/la00070a008>.
- [58] C.-H. Chang, E.I. Franses, Adsorption dynamics of surfactants at the air/water interface: a critical review of mathematical models, data, and mechanisms, *Colloids Surf. A Physicochem. Eng. Asp.* 100 (1995) 1–45, [https://doi.org/10.1016/0927-7757\(94\)03061-4](https://doi.org/10.1016/0927-7757(94)03061-4).
- [59] D. Attwood A.T. Florence Surfactant Systems: Their chemistry, pharmacy and biology 1st edition, 1983 Chapman & Hall London 10.1007/978-94-009-5775-6.
- [60] L.-J. Chen, S.-Y. Lin, C.-C. Huang, Effect of Hydrophobic Chain Length of Surfactants on Enthalpy–Entropy Compensation of Micellization, *J. Phys. Chem. B* 102 (1998) 4350–4356, <https://doi.org/10.1021/jp9804345>.
- [61] E. Mohajeri, G.D. Noudeh, Effect of Temperature on the Critical Micelle Concentration and Micellization Thermodynamic of Nonionic Surfactants: Polyoxyethylene Sorbitan Fatty Acid Esters, *J. Chem.* 9 (2012) 2268–2274, <https://doi.org/10.1155/2012/961739>.
- [62] P. Kroll, J. Benke, S. Enders, C. Brandenbusch, G. Sadowski, Influence of Temperature and Concentration on the Self-Assembly of Nonionic CIEJ Surfactants: A Light Scattering Study, *ACS Omega* 7 (2022) 7057–7065, <https://doi.org/10.1021/acsomega.1c06766>.
- [63] J.M. Corkill, J.F. Goodman, R.H. Ottewill, Micellization of homogeneous non-ionic detergents, *Trans. Faraday Soc.* 57 (1961) 1627, <https://doi.org/10.1039/ft9615701627>.
- [64] K. Shinoda, T. Nakagawa, B.-I. Tamamushi, T. Isemura, *Colloidal Surfactants: Some Physicochemical Properties*, Academic Press, New York, 1963.
- [65] C. Tanford, *The hydrophobic effect: Formation of micelles and biological membranes*, Wiley, 1980.
- [66] D. Cholokova, N. Denkov, Rotator phases in alkane systems: In bulk, surface layers and micro/nano-confinements, *Adv. Colloid Interface Sci.* 269 (2019) 7–42, <https://doi.org/10.1016/j.cis.2019.04.001>.
- [67] F. Guay, S. Bisailon, Validation of a mathematical model using the computer for the evaluation of different parameters related to interfaces of air/water and soyabean oil/water systems, *J. Colloid Interface Sci.* 93 (1983) 25–32, [https://doi.org/10.1016/0021-9797\(83\)90380-6](https://doi.org/10.1016/0021-9797(83)90380-6).
- [68] F. Liu, Z. Wang, D. Sun, X. Wei, W. Zhou, G. Li, G. Zhang, Adsorption kinetics of Brij 97 at the air/aolution interface, *J. Dispersion Sci. Techn.* 27 (2006) 657–663, <https://doi.org/10.1080/019326906006060624>.
- [69] K. Risse, S. Drusch, (Non)linear interfacial rheology of Tween, Brij and Span stabilized oil–water interfaces: Impact of the molecular structure of the surfactant on the interfacial layer stability, *Langmuir* 40 (2024) 18283–18296, <https://doi.org/10.1021/acs.langmuir.4c02210>.
- [70] L. Qin, X.-H. Wang, Surface adsorption and thermodynamic properties of mixed system of ionic liquid surfactants with cetyltrimethyl ammonium bromide, *RSC Adv.* 7 (2017) 51426–51435, <https://doi.org/10.1039/c7ra08915e>.
- [71] R. Miller, V.B. Fainerman, Thermodynamics and kinetics of protein/surfactant mixtures adsorbed at liquid interfaces, in: *Molecular Interfacial Phenomena of Polymers and Biopolymers*, Elsevier, 2005: pp. 3–47. 10.1533/9781845690830.1.3.
- [72] M. Mulqueen, K.J. Stebe, D. Blankshtein, Dynamic Interfacial Adsorption in Aqueous Surfactant Mixtures: Theoretical Study, *Langmuir* 17 (2001) 5196–5207, <https://doi.org/10.1021/la0103923>.
- [73] Ch. Ybert, J.-M. di Meglio, Study of Protein Adsorption by Dynamic Surface Tension Measurements: Diffusive Regime, *Langmuir* 14 (1998) 471–475, <https://doi.org/10.1021/la970999c>.
- [74] S. Rouimi, C. Schorsch, C. Valentini, S. Vaslin, Foam stability and interfacial properties of milk protein–surfactant systems, *Food Hydrocoll.* 19 (2005) 467–478, <https://doi.org/10.1016/j.foodhyd.2004.10.032>.
- [75] N.C. Christov, K.D. Danov, P.A. Kralchevsky, K.P. Ananthapadmanabhan, A. Lips, Maximum Bubble Pressure Method: Universal Surface Age and Transport Mechanisms in Surfactant Solutions, *Langmuir* 22 (2006) 7528–7542, <https://doi.org/10.1021/la061239h>.
- [76] K. Golemanov, N.D. Denkov, S. Tcholakova, M. Vethamuthu, A. Lips, Surfactant Mixtures for Control of Bubble Surface Mobility in Foam Studies, *Langmuir* 24 (2008) 9956–9961, <https://doi.org/10.1021/la8015386>.
- [77] K.G. Marinova, N.D. Denkov, Foam Destruction by Mixed Solid–Liquid Antifoams in Solutions of Alkyl Glucoside: Electrostatic Interactions and Dynamic Effects, *Langmuir* 17 (2001) 2426–2436, <https://doi.org/10.1021/la001558n>.
- [78] K.D. Danov, T.D. Gurkov, T. Dimitrova, I.B. Ivanov, D. Smith, Hydrodynamic Theory for Spontaneously Growing Dimple in Emulsion Films with Surfactant Mass Transfer, *J. Colloid Interface Sci.* 188 (1997) 313–324, <https://doi.org/10.1006/jcis.1997.4719>.
- [79] V. Chandran Suja, A. Kar, W. Cates, S.M. Remmert, P.D. Savage, G.G. Fuller, Evaporation-induced foam stabilization in lubricating oils, *Proc. Natl. Acad. Sci. U.S.A.* 115 (2018) 7919–7924, <https://doi.org/10.1073/pnas.1805645115>.
- [80] C.G. Malmberg, A.A. Maryott, Dielectric constant of water from 0° to 100° C, *J. RES. NATL. BUR. STAN.* 56 (1956) 1, <https://doi.org/10.6028/jres.056.001>.
- [81] I. Thormählen, J. Straub, U. Grigull, Refractive Index of Water and Its Dependence on Wavelength, Temperature, and Density, *J. Phys. Chem. Ref. Data* 14 (1985) 933–945, <https://doi.org/10.1063/1.555743>.
- [82] C. Márquez-Beltrán, D. Langevin, Electrostatic effects in films stabilised by non-ionic surfactants, *J. Colloid Interface Sci.* 312 (2007) 47–51, <https://doi.org/10.1016/j.jcis.2006.10.015>.
- [83] P.R. Garrett, P.R. Moore, Foam and dynamic surface properties of micellar alkyl benzene sulphonates, *J. Colloid Interface Sci.* 159 (1993) 214–225, <https://doi.org/10.1006/jcis.1993.1315>.
- [84] S. Tcholakova, B. Petkova, Bubble size and foamability: Role of surfactants and hydrodynamic conditions, *Curr. Opin. Colloid Interf. Sci.* 72 (2024) 101824, <https://doi.org/10.1016/j.cocis.2024.101824>.
- [85] H.M. Princen, The structure, mechanics, and rheology of concentrated emulsions and fluid foams. In *Encyclopedia of Emulsion Science and Technology*. J. Söblom, Ed.; Marcel Dekker: New York, 2001, Chapter 11.
- [86] S. Tcholakova, F. Mustan, N. Pagureva, K. Golemanov, N.D. Denkov, E.G. Pelan, S. D. Stoyanov, Role of surface properties for the kinetics of bubble Ostwald ripening in saponin-stabilized foams, *Colloids Surf. A Physicochem. Eng. Asp.* 534 (2017) 16–25, <https://doi.org/10.1016/j.colsurfa.2017.04.055>.
- [87] I. Lesov, S. Tcholakova, M. Kovadjieva, T. Saison, M. Lamblet, N. Denkov, Role of Pickering stabilization and bulk gelation for the preparation and properties of solid silica foams, *J. Colloid Interface Sci.* 504 (2017) 48–57, <https://doi.org/10.1016/j.jcis.2017.05.036>.
- [88] S. Tcholakova, Z. Mitrinova, K. Golemanov, N.D. Denkov, M. Vethamuthu, K. P. Ananthapadmanabhan, Control of Ostwald Ripening by Using Surfactants with High Surface Modulus, *Langmuir* 27 (2011) 14807–14819, <https://doi.org/10.1021/la203952p>.
- [89] F. Mustan, N. Politova-Brinkova, D. Rossetti, P. Rayment, S. Tcholakova, Oil soluble surfactants as efficient foam stabilizers, *Colloids Surf. A Physicochem. Eng. Asp.* 633 (2022) 127874, <https://doi.org/10.1016/j.colsurfa.2021.127874>.
- [90] V.M. Sadtler, M. Guey, P. Marchal, L. Choplin, Shear-induced phase transitions in sucrose ester surfactant, *J. Colloid Interface Sci.* 270 (2004) 270–275, <https://doi.org/10.1016/j.jcis.2003.10.038>.
- [91] A. Rezaei, Z. Derikvand, R. Parsaei, M. Imanivarnosfaderani, Surfactant-silica nanoparticle stabilized N2-foam flooding: A mechanistic study on the effect of surfactant type and temperature, *J. Mol. Liq.* 325 (2021) 115091, <https://doi.org/10.1016/j.molliq.2020.115091>.
- [92] K. Oetjen, C. Bilke-Krause, M. Madani, T. Willers, Temperature effect on foamability, foam stability, and foam structure of milk, *Colloids Surf. A Physicochem. Eng. Asp.* 460 (2014) 280–285, <https://doi.org/10.1016/j.colsurfa.2014.01.086>.
- [93] G.D. Burnett, J.J. Chae, W.Y. Tam, R.M. de Almeida, M. Tabor, Structure and dynamics of breaking foams, *Phys Rev E* 51 (1995) 5788–5796, <https://doi.org/10.1103/physreve.51.5788>.
- [94] J.J. Chae, M. Tabor, Dynamics of foams with and without wall rupture, *Phys. Rev. E* 55 (1997) 598–610, <https://doi.org/10.1103/PhysRevE.55.598>.
- [95] A. Hasmy, R. Paredes, O. Sonneville-Aubrun, B. Cabane, R. Botet, Dynamical Transition in a Model for Dry Foams, *Phys. Rev. Lett.* 82 (1999) 3368–3371, <https://doi.org/10.1103/PhysRevLett.82.3368>.
- [96] E. Carey, C. Stubenrauch, Free drainage of aqueous foams stabilized by mixtures of a non-ionic (C12DMPO) and an ionic (C12TAB) surfactant, *Colloids Surf. A Physicochem. Eng. Asp.* 419 (2013) 7–14, <https://doi.org/10.1016/j.colsurfa.2012.11.037>.
- [97] V. Carrier, A. Colin, Coalescence in Draining Foams, *Langmuir* 19 (2003) 4535–4538, <https://doi.org/10.1021/la026995b>.
- [98] V. Carrier, S. Destouesse, A. Colin, Foam drainage: A film contribution? *Phys. Rev. E* 65 (2002) 061404 <https://doi.org/10.1103/PhysRevE.65.061404>.
- [99] S.J. Neethling, J.J. Cilliers, Modelling flotation froths, *International Journal of Mineral Processing* 72 (2003) 267–287, [https://doi.org/10.1016/S0301-7516\(03\)00104-2](https://doi.org/10.1016/S0301-7516(03)00104-2).

## Further reading

- [100] Z. Briceño-Ahumada, W. Drenckhan, D. Langevin, Coalescence in Draining Foams Made of Very Small Bubbles, *Phys. Rev. Lett.* 116 (2016) 128302, <https://doi.org/10.1103/PhysRevLett.116.128302>.